Master Thesis

Study of the transport properties of hydrogen in aqueous solutions at conditions relevant to underground hydrogen storage

Ke Xu

Delft University of Technology

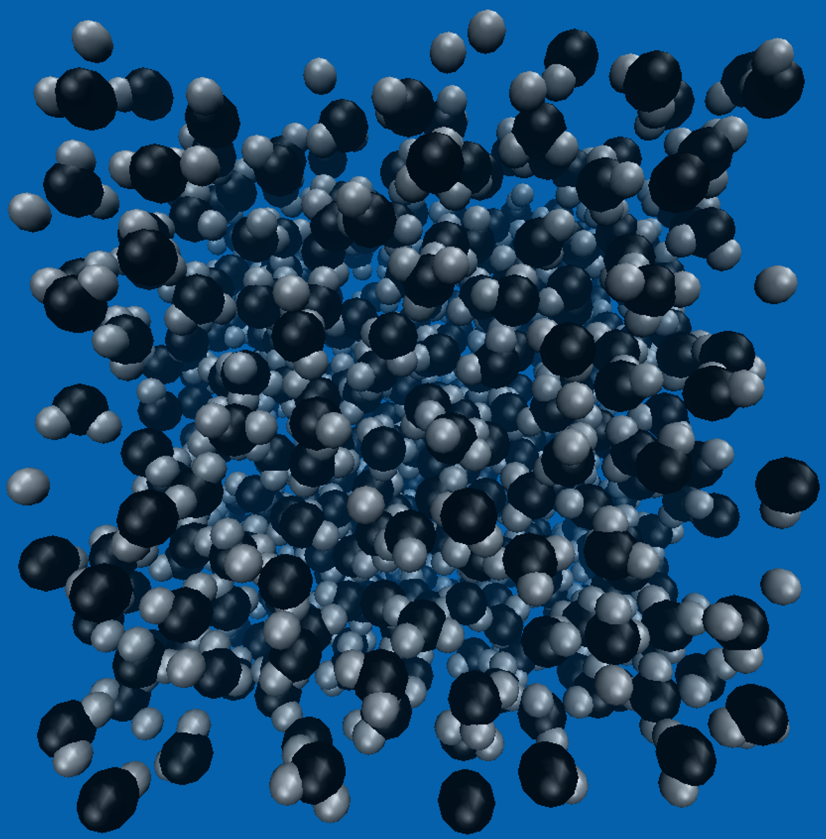

TU Delft

Master Thesis

Study of the transport properties of hydrogen in aqueous solutions at conditions relevant to underground hydrogen storage

by

Ke Xu

Student Name	Student Number
Ke Xu	5354986

Instructor:	Poulumi Dey
	Othonas Moultos
Daily Supervisor:	Parsa Habibi
Committee member:	Poulumi Dey
	Othonas Moultos
	Mahinder Ramdin
Project Duration:	Nov, 2021 - July, 2022
Faculty:	Faculty of Mechanical, Maritime and Materials Engineering (3mE), Delft

Cover: 500 water molecules created by VMD software (Modified)

TU Delft

Abstract

Hydrogen has been deemed an appealing energy source with tremendous promise as a method to minimize dependency on imported non-renewable energy sources. However, the optimum approach for storing hydrogen on an industrial scale is still currently being researched. A substantial volume of hydrogen stored in the mid to long term as a surplus energy source is still critical to meeting the massive demand at a reduced cost. Underground hydrogen storage is thus being considered for development, despite the fact that it currently still faces several hurdles. Because of its high diffusion coefficient, hydrogen leaking to the surface is one of the most serious issues with underground hydrogen storage. It is more diffusive over overburden strata than air, carbon dioxide, or methane because of its low molar weight. Hydrogen has a diffusion coefficient three times larger than methane in pure water at normal temperature and pressure. The lack of data on hydrogen diffusion coefficients in diverse solutions at high pressures and temperatures, on the other hand, continues to stymie future study.

Molecular dynamics simulations are becoming more popular since they are a faster and more convenient approach that may also produce findings with difficult-to-perform circumstances. At various temperatures and pressures, the transport properties of hydrogen in aqueous solutions are estimated using molecular dynamics simulations. The density, shear viscosity, and self-diffusion coefficient were explored using LAMMPS for on-the-fly computation of transport properties of fluids with the Order-n algorithm. The calculating outputs are compared to the experimental data to determine the method's dependability. The selection of the forcefields of water, hydrogen, and ions, as well as the impact of pressure and temperature, are explored based on the results. Also included are density, shear viscosity, and diffusion coefficient values at high pressures up to 1000bar and 723K which give a sufficient dataset for the these properties of hydrogen in NaCl systems.

Contents

Nomenclature

Abbreviations

Abbreviation	Definition
LAMMPS	Large-scale Atomic/Molecular Massively Parallel Simulator
OCTP	On-the-fly calculation of transport properties
GHG	Greenhouse gases
UHS	Underground hydrogen storage

Symbols

Symbol	Definition	Unit
T	Temperature	[K]
P	Pressure	[bar]
m	Molality	[mol/kg]
D_w	Diffusion coefficient of water	[m^2/s]
D_{Na^+}	Diffusion coefficient of Na^+	[m^2/s]
D_{Cl^-}	Diffusion coefficient of Cl^-	[m^2/s]
D_{H}	Diffusion coefficient of H_2	[m^2/s]
D_{H_w}	Diffusion coefficient of H_2 in water	[m^2/s]
ρ	Density	[kg/m^3]
η	Shear viscosity	[mPas]
σ_ρ	Stand deviation of density	[kg/m^3]
σ_η	Stand deviation of viscosity	[mPas]
σ_{Dw}	Stand deviation of diffusion coefficient of water	[m^2/s]
σ_{DNa^+}	Stand deviation of diffusion coefficient of Na^+	[m^2/s]
σ_{DCl^-}	Stand deviation of diffusion coefficient of Cl^-	[m^2/s]
σ_{DH}	Stand deviation of diffusion coefficient of H_2	[m^2/s]
σ_{DH_w}	Stand deviation of diffusion coefficient of H_2 in water	[m^2/s]

1

Introduction

In aqueous solutions, hydrogen diffusivity is found in a range of environmental, geological, industrial, and biological systems. The diffusion process of light, low solubility gas in aqueous solutions, for example, is a critical controlling parameter during air-water gas exchange. Fuel cells and electrolysis are examples of industrial applications that use hydrogen diffusion at low to moderate temperatures.

The intradiffusion coefficients of H_2 in different kinds of aqueous solutions across a wide variety of circumstances, including gas, liquid, and supercritical, are required for the design and optimization of these engineering processes. Various studies have been carried out throughout the years in order to get precise data regarding hydrogen diffusivity in various types of aqueous solutions. For example, when it comes to the underground hydrogen storage, the diffusivity of the hydrogen in the aqueous solutions is quite essential to study.

Among existing renewable energy sources, primarily fossil-based such as oil, hydrogen has been deemed an appealing renewable energy source with tremendous promise as a method to minimize dependency on imported non-renewable energy sources. In order to satisfy international climate protection agreements[1], the use of hydrogen energy and its related technical research has attracted a lot of attention. The diffusivity of hydrogen in the aqueous solution can determine the storage method, the materials selections when it comes to the hydrogen storage. The optimum approach for storing hydrogen on an industrial scale is still currently being researched. A substantial volume of hydrogen stored in the mid to long term as a surplus energy source is still critical to meeting the massive demand (either as a buffer for seasonal demand or completely) at a reduced cost. Underground hydrogen storage is thus being considered for development, despite the fact that it currently faces several hurdles. Because of its high diffusion coefficient, hydrogen leaking to the surface is one of the most serious issues with underground hydrogen storage. It is more diffusive over overburden strata than air, carbon dioxide, or methane because to its low molar weight.

However, because to the experimental limitations, the state points can only give a narrow scope for the entire system[2]. Data points with high molalities, high temperatures, and high pressures are difficult to find, and it is hard to conduct experiments under these conditions. As a result, a simulation of the process is required to supplement the data.

Molecular dynamics simulation is considered to use. Molecular dynamics is a computer simulation approach for studying atoms and molecules' physical motions. The atoms and molecules are allowed to interact for a certain amount of time, providing a perspective of the system's dynamic evolution.In the most common version, the trajectories of atoms and molecules are calculated by numerically solving Newton's equations of motion for a system of interacting particles, with forces between the particles and potential energies calculated using interatomic potentials or molecular mechanics force fields[3].

The simulation of hydrogen diffusivity in aqueous solutions systems is therefore created in order to get a dataset of the systems that spans the liquid and supercritical states. LAMMPS(Large-scale Atomic/-

Molecular Massively Parallel Simulator) is used for the simulation[4]. LAMMPS is a classical molecular dynamics (MD) programme that simulates particle ensembles in liquid, solid, or gaseous states. Using a range of interatomic potentials (force fields) and boundary conditions, it may mimic atomic, polymeric, biological, solid-state (metals, ceramics, oxides), granular, coarse-grained, or macroscopic systems. It can simulate 2D or 3D systems with as little as a few particles or as many as millions or billions.

Jamali et al.[5] has created a tool for on-the-fly calculation of transport properties(OCTP) of fluids with the order-n algorithm in LAMMPS. In a single simulation, OCTP computes the self- and MaxwellStefan diffusivities, bulk and shear viscosities, and thermal conductivities of pure fluids and mixtures. OCTP is the first LAMMPS implementation to employ Einstein relations in conjunction with the order-n technique for efficient sampling of dynamic variables. The characteristics of fluids and gases in many types of systems can be estimated using different forcefields.

In order to calculate the thermodynamic and transport properties of aqueous solutions, the systems is determined for different components. Thus, the selected systems which is needed to be explored are listed below:

- H_2/H_2O/NaCl

The aim of this project is to investigate the transport properties of hydrogen in different kinds of aqueous solutions under various pressures and temperatures. By running the simulations at different conditions, the new combination of ions forcefields, hydrogen model and water model are tested and validated. Molality, pressure and temperature effect are compared and the transport properties' data of these pressure and temperature set are provided.

The main methodology including the force field model and the main equations are studied in the next sections. The basic properties including density, shear viscosity of the different systems and also the diffusion coefficient of different components are calculated in the following sections with comparison to the experimental data in order to show the results of the combining forcefields.

2

Literature review

In this chapter, the current research of underground hydrogen storage as well as the transport properties of hydrogen in the aqueous solutions will be given. To gain a broader understanding of the problem, the current ways to investigate the transport properties will be listed and discussed. Moreover, the related background knowledge, the analysis of the issue and also the research questions will be shown in the following sections.

2.1. Underground hydrogen storage

Renewable energy sources are gaining popularity as an alternative to fossil fuel-based energy sources in order to satisfy international climate protection agreements. This is because it emits only trace amounts of greenhouse gases (GHG) and hence aids in the fight against climate change caused by the use of fossil fuels[1].

Among existing renewable energy sources, such as solar and wind energy, which are extremely weather dependent, hydrogen has been considered an appealing renewable energy source with great potential as a way to reduce reliance on imported non-renewable energy sources, particularly fossil-based such as oil. Aside from its multiple applications such as propelling fuel, fuel cell, agriculture, and refinery, hydrogen has been demonstrated as a secondary source of energy as a significant energy carrier[6]. Furthermore, the variability of most renewable sources is a significant drawback that can result in momentary mismatches between demand and supply. As a result, one possibility for closing the energy gap is to convert excess energy into hydrogen and store it underground.

Hydrogen may be created by a variety of mechanisms, including thermochemical, electrolytic, biological, and direct solar water splitting. The hydrogen produced can be stored using a variety of methods, including high-pressure gas cylinders, cryogenic tanks, adsorbed hydrogen on materials with a high specific surface area, absorbed on interstitial sites in a host metal, chemically bonded in covalent and ionic compounds, and oxidation of reactive metals, such as Li, Na, Mg, Al, and Zn with water[1].

Nowadays, mid- to long-term storage of a massive quantity of hydrogen as a surplus energy source is still critical to meeting the increasing demands (either as a buffer for seasonal demand or in its entirety) at a reduced cost. However, hydrogen storage in geological formations (porous medium) such as below depleted oil and gas reserves, aquifers, or cavern storage has made it practical (excavated or solution mined rocks such as salt coal, igneous and metamorphic rocks).

According to Taylor et al. (1986), underground storage is the cheapest method for storing large quantities of gaseous hydrogen[7]. However, due to hydrogen's low density, viscosity, and molecular size, leakage and therefore hydrogen loss are widespread and significant issues that must be addressed. It has been discovered that UHS is very similar to underground natural gas storage, and most past and ongoing underground hydrogen projects use underground natural gas storage experiences in every aspect, such as site specifications, storage techniques, monitoring, and even cost life cycle or economic

viability. The main distinction is that the physical and chemical properties of hydrogen and natural gas require more attention, particularly in terms of leakage, monitoring, and chemical affinity, which makes hydrogen more active to proceed for chemical, biological, or microbial reactions, resulting in hydrogen loss and thus energy. Again, physical features like as low viscosity and great mobility result in atypical hydrodynamic behavior[1].

Because fluid saturation changes throughout each storage and withdrawal cycle, flow behavior studies are recommended for each cycle. The flow behavior is also affected by viscosity, density, gravitational and viscous forces, as well as flow direction, which influences hydrogen storage efficiency [8]. The imbalance of active forces in the reservoir, together with the high injection rate, may cause fingering and impact the different hydrogen losses[9].

In the recent decade, there has been a lot of interest on hydrogen storage, particularly underground storage (because to its large capacity and cheaper cost) as energy storage and in the path to the success of the fossil to renewable energy revolution. Several projects such as Roads2HyCOM (2005)[10], Hychico (2006)[11], H2STORE (2012)[12], HyUnder (2012)[13] and HyINTEGER (2016)[14] were created to investigate the feasibility in terms of production, transportation, storage and utilization of hydrogen in the last decade. But as mentioned above, the physical properties especially the transport properties of hydrogen in water and other aqueous solutions under high pressures and high temperatures are still urgently needed to better develop the further design of the UHS projects.

2.2. Transport properties

This section introduces the fundamentals of transport characteristics, namely density, shear viscosity and the self diffusion coefficient. Other calculation theories are widely utilized while measuring the system, in addition to setting experiments for the observations of these features.

2.2.1. Density

The density of a substance is its mass per unit volume.

Following table 2.1 is the data that was investigated by Manohar et al.[15] which contains the data under the temperature up to 413K for low concentrations of NaCl. The density of aqueous electrolyte solution of NaCl was measured by Green et al.[16] over a temperature range from 273.15K to 373.15K. The mass fraction of NaCl range from 1% to 26% and the pressure of the measurement is 1 bar. The detailed data of the density of NaCl is as table2.2 shows.

The current literature data measuring the density of the NaCl solutions are quite limited by the molality and the temperatures. Also, most of the data are measured under 1bar, without considering the pressure effect to the whole system. The sufficient data of various molalities at certain temperatures are hard to find, especially when it comes to high temperatures and high molalities.

Table 2.1: Density of NaCl solutions from 298K to 413K [15]

Molality	Temperature[K]					
	298	308	318	353	373	413
1	1036.14	1032.56	1028.18	1009.07	995.967	965.093
2.5	1089.36	1085.03	1079.92	1060.18	1047.14	1017.76
4	1152	1147.12	1141.33			

Table 2.2: Density of NaCl solutions from 273.15K to 373.15K [16]

NaCl mass fraction	c(NaCl)*	ρ [g.cm^{-3}]					
%	mol/L	288.15K	293.15K	303.15K	333.15K	353.15K	373.15K
1	0.1724	1.00707	1.00409	0.99908	0.9900	0.9785	0.9651
2	0.3474	1.01442	1.01112	1.00593	0.9967	0.9852	0.9719
4	0.7052	1.0292	1.0253	1.01977	1.0103	0.9988	0.9855
8	1.4526	1.05907	1.05412	1.04798	1.0381	1.0264	1.0134
12	2.2431	1.08946	1.08365	1.07699	1.0667	1.0549	1.0420
16	3.0777	1.12056	1.11401	1.10688	1.0962	1.0842	1.0713
20	3.9581	1.15254	1.14533	1.13774	1.1268	1.1146	1.1017
24	4.8868	1.18557	1.17776	1.16971	1.1584	1.1463	1.1331
26	5.3701	1.20254	1.19443	1.18614	1.1747	1.1626	1.1492

* The number of this column is calculated by the data from mass fraction and the density.

2.2.2. Viscosity

Viscosity, a sort of internal friction, is present in all common fluids. A constant force is required to keep a fluid flowing, just as a constant force is required to keep a solid body moving in the presence of friction. The SI units of viscosity η are N·s/m^2 or Pa·s. In general, viscosity is affected by a fluid's condition, such as temperature, pressure, and rate of deformation. However, in certain circumstances, the dependency on some of these qualities is insignificant.

Shear viscosity is one of the liquid transport coefficients that characterizes the transverse momentum current[17]. It is vital in tackling flows in chemical engineering, mechanical engineering, geophysics, and other domains since it regulates the macroscopic flow of liquids. Furthermore, a solvent's shear viscosity is sometimes viewed as a measure of the rates of dynamic processes of solutes dispersed in the solvent.

Using the classical method as experiments to test the viscosity is widely accepted in the last century. From the following table 2.3 the viscosity data of the NaCl solution is provided. But because of the limitation of the temperatures and molalities, the data is not that sufficient.

Table 2.3: Viscosity of NaCl solutions from 303K to 328K [18]

Molality	Temperature[K]					
	303	308	313	318	323	328
1	0.88242	0.7851	0.72047	0.65892	0.60847	0.56095
1.5	0.91829	0.8232	0.75506	0.69169	0.63799	0.58967
2	0.96612	0.86778	0.79878	0.72922	0.67517	0.62294
2.5	1.02351	0.9181	0.84186	0.77033	0.71234	0.65923
3	1.08091	0.97346	0.89602	0.8174	0.75444	0.69602
3.5	1.14308	1.02091	0.93909	0.8597	0.79216	0.73079
4	1.21323	1.08274	0.99913	0.90676	0.83699	0.77262
4.5	1.28656	1.15248	1.05395	0.96455	0.88619	0.81899
5	1.36229	1.23301	1.12639	1.03128	0.94523	0.86939

Several empirical/semi-empirical models for forecasting shear viscosity have been developed, including free-volume theory[19], friction theory[20], and functional form fitting[21]. Shear viscosity may also be calculated using equilibrium or nonequilibrium molecular dynamics (MD) simulations. The shear viscosity in equilibrium MD (EMD) may be calculated using the Einstein relation:

$$\eta = \lim_{t\to\infty} \frac{1}{10\cdot 2t}\frac{V}{k_B T}\left\langle \sum_{\alpha\beta}\left(\int_0^t P_{\alpha\beta}^{os}\left(t'\right)\mathrm{d}t'\right)^2\right\rangle \tag{2.1}$$

where

$$P_{\alpha\beta}^{os} = \frac{P_{\alpha\beta} + P_{\beta\alpha}}{2} - \delta_{\alpha\beta}\left(\frac{1}{3}\sum_{k} P_{kk}\right) \tag{2.2}$$

where η is the shear viscosity, V is the volume of the system, k_B is the Boltzmann constant, $P_{\alpha\beta}^{os}$ denotes the components of the traceless pressure tensor, $P_{\alpha\beta}$ denotes the off-diagonal components of the pressure tensor, and $\delta_{\alpha\beta}$ is the Kronecker delta. $\langle ... \rangle$ indicates an ensemble average.

Also, Green-Kubo formula is also a commonly choice when calculating the shear viscosity of the system. According to the Kubo−Green formula, the steady-state shear viscosity of liquid, denoted as η_0, is described in terms of the time-correlation function of the anisotropic part of the stress tensor, $\mathrm{P}^{(s)}$, as:

$$\eta_0 = \frac{V}{k_B T}\int_0^{\infty} \mathrm{d}t \left\langle P_{xz}^{s}(0)\, P_{xz}^{s}(t)\right\rangle \tag{2.3}$$

where k_B and T stand for the Boltzmann constant and the absolute temperature, respectively. Equation 2.3 states that the steady-state shear viscosity is determined by the dynamics of the stress tensor.

Using the Einstein relation in calculating the transport properties can provide a criterion for defining the minimum simulation length for obtaining a transport property. When the slope of linear relationship between time and the mean-squared displacement in the log-log plot reaches 1, the dynamical properties of interest is valid at timescales[22].

2.2.3. Diffusion coefficient

Diffusion coefficient is the proportionality factor D in Fick's law. As a result, the diffusion coefficient suggests that the substance's mass diffuses over a unit surface in a unit time with a concentration gradient of unity. In the SI system, D is defined as a square meter per second. The diffusion coefficient is a physical constant that is affected by molecule size, other characteristics of the diffusing material, temperature, and pressure. The diffusion coefficients of one substance into another are often calculated.

According to IUPAC definition[23], when the chemical potential gradient is zero, the self-diffusion coefficient is the diffusion coefficient D_i of species i. Self diffusion coefficient can be calculated when there is no experimental data. There are two widely used approaches for calculating transport properties of equilibrium systems from molecular dynamics (MD) simulations. The first one is based on the Gree-Kubo formula. The self-diffusion coefficient can be computed from the velocity autocorrelation function by the Green-Kubo formula.

$$D = \lim_{t\to\infty} D_{GK}(t) \tag{2.4}$$

$$D_{GK}(t) = \frac{1}{3N}\sum_{i=1}^{N}\int_0^t < \mathbf{v}_i(\tau)\cdot\mathbf{v}_i(0)\, d\tau \tag{2.5}$$

where $v_i(\tau)$ is the velocity of nucleus i at time τ , and an average over the particles is performed to improve statistical precision[24].

It is also possible to do the calculation of the self diffusion coefficient using Einstein relation[22]. The related equation of self diffusion coefficient is shown in eqs 2.6.

$$D_i = \lim_{t\to\infty}\frac{1}{6N_i t}\left\langle \sum_{j=1}^{N_i}\left(r_{j,i}(t) - r_{j,i}(0)^2\right)\right\rangle \tag{2.6}$$

where D_i is the self-diffusivity (or intradiffusivity in the case of mixtures) of species $i, r_{j,i}(t)$ is the position of the jth molecule of species i at time t, and N_i is the number of molecules of species i in the system.

Similar as the calculation of the shear viscosity of the system, When applying the Einstein relation, the slope of the linear connection between time and the mean-squared displacement in the log-log plot may simply assist to identify whether the simulation runs for enough time to obtain the final conclusion.

3

Methodology

The methodology of the project can basically introduced in the following parts. The first part is the force fields. The second part is the molecular dynamics details and the following is the main equations that is needed in the simulations to do the computation of transport properties.

3.1. Forcefield data

A force field is a computational tool used in chemistry and molecular dynamics to estimate the forces between atoms within molecules as well as between molecules. In molecular mechanics, molecular dynamics, or Monte Carlo simulations, the force field refers to the functional form and parameter settings used to determine the potential energy of a system of atoms or coarse-grained particles. The parameters for a given energy function might be generated via physics and chemistry experiments, quantum mechanics calculations, or a combination of both[3].

Different kinds of simulation models are used to measure the components that is functioned in the whole force field. In this study, the TIP4P/2005 model[25] was employed, which is a generic parameterization for modeling the full phase diagram of condensed water. For modeling H_2, the force fields developed by Vrabec et al.[26] is used. To model Sodium ion , Potassium ion and Chloride ion, the force fields developed by Madrid[27] is used. The charge of the model is from Madrid[27], the fitted parameter is changed.

Table 3.1 lists the chemical substances used in this study for molecular simulation.

Table 3.1: Chemical Substances Used for Molecular Simulation

Componet	Chemical formula	CAS number	Forcefield
Water	H_2O	7732-18-5	TIP4P/2005 [25]
Hydrogen	H_2	133-74-0	Vrabec [26]
Sodium ion	Na^+	7440-23-5	Madrid [27]
Chloride ion	Cl^-	7782-50-5	Madrid [27]

3.1.1. Water model

A water model is used in computational chemistry to simulate and calculate the thermodynamics of water clusters, liquid water, and aqueous solutions with specified solvent. To create this model, different kinds of knowledge are required including quantum mechanics, molecular mechanics, experimental data, and the combinations of these.

To categorized these models, there are three things that is need to be considered:

- the number of interaction points
- whether the model is rigid or flexible
- whether the model includes polarization effect

Three site water model
Three-site models have three interaction points corresponding to the three atoms of the water molecule. Each site has a point charge, and the site corresponding to the oxygen atom also has the Lennard-Jones parameters. TIPS, SPC and IP3P are commonly used three-site models.

SPC/E water model is one of the three-site models of water. The shear viscosity for the SPC/E model

Table 3.2: Parameters of the SPC/E water model

r(OH)(Å)	HOH(°)	σ(Å)	ϵ(kJ/mol)	q(H)(e)	q(O)(e)
1.0	109.47	3.166	0.650	0.4238	−0.8476

is 0.729 mPa.s at 298 K and 1 bar[28] (experimental value 0.896 mPa.s[29]).

Four site water model
The four-site models have four interaction points by adding one dummy atom near of the oxygen along the bisector of the H-O-H angle of the three-site models. The dummy atom M only has a negative charge. The TIP4P/2005 is one of the four site model of water models. TIPS2, TIP4P, and TIP4P-Ew are also typical selections as the four site water models.

The TIP4P/2005 model consists of a Lennard-Jones site for the oxygen atom, and three charge sites.

Table 3.3: Parameters of the TIP4P/2005 water model

r(OH)[Å]	HOH[°]	σ[Å]	ϵ/k_B[K]	q(H)[e]	q(M)[e]	r(OM)[Å]
0.9572	104.52	3.1589	93.2	0.5564	−1.1128	0.1546

The TIP4P/2005 potential has a self-diffusion coefficient, in bulk water at 298 K, of 0.21 $Å^2 \cdot ps^{-1}$ in a classical simulation of 216 water molecules (experimental value: 0.23 $Å^2 \cdot ps^{-1}$)[30]. The shear viscosity for the TIP4P/2005 model is 0.855 mPa·s at 298 K and 1 bar[28] (experimental value 0.896 mPa·s[29]).

3.1.2. Hydrogen model

Single site hydrogen model
Typical single site hydrogen model consitis of the model created by Vrabec et al[26], Buch[31] and so on. In table3.4 the detailed information of the Vrabec model for hydrogen is given. This model is created by Vrabec et al.[26], which is aimed for the better study of the thermodynamics properties including the phase behavior of all mixtures containing hydrogen, the main air components nitrogen, oxygen, and argon, as well as water. The H-H bond length of the force filed is 0.74 Å.

Table 3.4: Parameters for the hydrogen model-Vrabec model

ϵ/k_B[K]	σ[Å]
25.84	3.0366

Two site hydrogen model
The hydrogen forcefield developed by Cracknell et al.[32] is the two site hydrogen model. A two-site model is simulated with the interactions summed over all site–site interactions.

Table 3.5: Parameters for the hydrogen model-Cracknell model

ϵ/k_B[K]	σ[Å]
12.5	2.59

Three site hydrogen model
Three site hydrogen model is the model with dummy site L as the geometric center of mass of the hydrogen. The modified three-site Silvera−Goldman by Alavi et al.[33], and Marx[34] are commonly used ones. The Marx model for hydrogen is one of the three-site hydrogen model created by Marx et al.[34] and his collegues in 1992. The H-H bond length of the force fields is 0.74 Å.

Table 3.6: Parameters for the hydrogen model-Marx model

ϵ/k_B[K]	σ[Å]	q_H[e]	q_L[e]
36.7	2.958	-0.936	0.468

3.1.3. Ions forcefield- madrid forcefield
The Madrid 2019 forcefield is created by Vega et al. and his colleagues[27]. The force field proposed is nonpolarizable, and both water molecules and sulfate anions are rigid. This forcefield is developed based on the TIP4P/2005 water model. Charges of 0.85 electron units are used to simulate monovalent ions. Up to large concentrations, the model enables a highly precise description of the solution densities. Viscosity up to 3mol/L concentrations may be accurately predicted by it as well.
Lennard-Jones parameters for NaCl solutions in TIP4P/2005 water in Madrid 2019 model is shown in Table 3.7.

Table 3.7: Lennard-Jones parameters for NaCl solutions in TIP4P/2005 water in Madrid-2019 model

interaction	Madrid Model	
	σ_{LJ}/nm	ϵ_{LJ}/(kJ/mol)
Na^+-Na^+	0.221737	1.472356
Cl^--Cl^-	0.469906	0.076923
Na^+-Cl^-	0.300512	1.438894
$Ow-Ow$	0.315890	0.774908
Na^+-Ow	0.260838	0.793388
Cl^--Ow	0.423867	0.061983

Based on the Madrid 2019 model, in order to have a better simulation results in the viscosity measurement, a new force field is created by Vega's group. In this new force field, monovalent ions is modeled using charges of 0.75 in electron units. Lennard-Jones parameters for NaCl and KCl solutions in TIP4P/2005 water in this new Madrid model are shown in Table 3.8.

Table 3.8: Lennard-Jones parameters for NaCl solutions in TIP4P/2005 water in the new Madrid model

interaction	Madrid Model	
	σ_{LJ}/nm	$\epsilon_{LJ}/$(kJ/mol)
Na^+-Na^+	0.221737	1.472356
Cl^--Cl^-	0.469906	0.076923
Na^+-Cl^-	0.258012	1.438894
$Ow-Ow$	0.315890	0.774908
Na^+-Ow	0.238725	0.793388
Cl^--Ow	0.407631	0.061983

3.2. Molecular Dynamics

Molecular dynamics is a computer simulation approach for studying atoms and molecules' physical motions. The atoms and molecules are allowed to interact for a certain amount of time, providing a perspective of the system's dynamic evolution. In the most common version, the trajectories of atoms and molecules are calculated by numerically solving Newton's equations of motion for a system of interacting particles, with forces between the particles and potential energies calculated using interatomic potentials or molecular mechanics force fields[3].

3.2.1. Design constraints

Under certain macroscopic conditions, a large number of independent systems with identical properties and structures in various motion states are called statistical ensembles, or ensembles for short. Each system in the ensemble is the same and under the same macroscopic conditions. An ensemble is a collection of systems. There are commonly used types of the ensembles.

- Microcanonical Ensemble (NVE): A micro-canonical ensemble, abbreviated as NVE, means that it has a certain number of particles (N), volume (V), and energy (E).
- Canonical Ensemble (NVT): A canonical ensemble, abbreviated as NVT, means that it has a certain number of particles (N), volume (V), and temperature (T).
- Isothermal and isobaric ensemble (NPT): The isothermal isobaric ensemble means that it has a certain number of particles (N), pressure (P), and temperature (T).

In order to control the temperature in the ensembles, there are several algorithm that can be used for constant temperature molecular dynamics simulations. For example, the Nosé–Hoover thermostat[35][36], Langevin thermostat[37] and Berendsen thermostat[38]. The volume of the simulated system is adjusted via barostats to regulate pressure. In practice, this is accomplished by scaling the coordinates of each atom in a system by a minor amount, causing the system's size to vary. The techniques of maintaining pressure are classified in the same way as temperature regulation is classified. Berendsen barostat, Parinello-Rahman barostat and Nose-Hoover barostat are commonly used ones for the pressure control.

Nosé-Hoover thermostat and barostat

The Nosé-Hoover thermostat is a deterministic technique for molecular dynamics simulations at constant temperature. It was created by Nosé and expanded upon by Hoover. Despite the fact that the Nosé-Hoover thermostat's heat bath is made up of only one fictitious particle, simulation systems attain realistic constant-temperature conditions (canonical ensemble). As a result, the Nosé-Hoover thermostat is widely utilized as one of the most precise and efficient approaches for constant-temperature molecular dynamics simulations. For the Nosé-Hoover barostat, Nose and Klein were the first to apply method analogous to Andersen's barostat for molecular simulation. This variation was further improved by Hoover. This is one of the two barostatting methods which are currently available in LAMMPS.

3.2.2. Potential functions

A potential function, or a description of the terms by which the particles in the simulation will interact, is required for a molecular dynamics simulation. The kinetic calculation is strongly connected to the

choosing of the action potential. The potential energy surface of the system will have distinct forms with different action potentials, and the trajectories of the molecular motion and intramolecular motion determined by the kinetic calculation will also be varied, affecting the sampling. The early molecular dynamics computation employed a rather basic rigid spherical potential, and now increasingly use the Lennard-Jones potential, which can better fit the interaction between particles. Following is the commonly used expression for Lennard-Jones potential.

$$V_{LJ}(r) = 4\varepsilon \left[\left(\frac{\sigma}{r}\right)^{12} - \left(\frac{\sigma}{r}\right)^{6} \right] \tag{3.1}$$

where r is the distance between two interacting particles, ε is the depth of the potential well (usually referred to as 'dispersion energy'), and σ is the distance at which the particle-particle potential energy V is zero (often referred to as 'size of the particle').

For the same kind of species, different kinds of forcefields are created to measure. The Lorentz−Berthelot combining rules are used for the interactions between unlike species.

Lorentz-Berthelot combining rules
Combining rules are equations in computational chemistry and molecular dynamics that provide the interaction energy between two distinct non-bonded atoms, often for the component of the potential reflecting the Van der Waals interaction.The selection of combining rules in the simulation of mixtures can occasionally alter the simulation's outcome.
H. A. Lorentz proposed the Lorentz rule in 1881:

$$\sigma_{ij} = \frac{\sigma_{ii} + \sigma_{jj}}{2} \tag{3.2}$$

The Berthelot rule (Daniel Berthelot, 1898) is given by:

$$\epsilon_{ij} = \sqrt{\epsilon_{ii} \cdot \epsilon_{jj}} \tag{3.3}$$

These are the most often used rules, and they are the default in many molecular modeling software.

3.2.3. Software

There are a lot of software that can be used for the molecular dynamics simulations, for example, GROMACS and LAMMPS.

GROMACS
GROMACS is a molecular dynamics software that primarily simulates proteins, lipids, and nucleic acids. It was created in the Biophysical Chemistry department of the University of Groningen. GROMACS is one of the most popular and quickest software packages available, and it can run on both central processing units (CPUs) and graphics processing units (GPUs) (GPUs).[39] It is a molecular dynamics simulation and energy-minimization engine.

LAMMPS
LAMMPS(Large-scale Atomic/Molecular Massively Parallel Simulator) is a classical molecular dynamics (MD) programme that simulates particle ensembles in liquid, solid, or gaseous states. Using a range of interatomic potentials (force fields) and boundary conditions, it may mimic atomic, polymeric, biological, solid-state (metals, ceramics, oxides), granular, coarse-grained, or macroscopic systems. It can simulate 2D or 3D systems with as little as a few particles or as many as millions or billions.

Although LAMMPS may be developed and run on a laptop or desktop computer, it is intended for parallel machines. It will operate in both serial and parallel mode on any system that supports the MPI message-passing library. Shared-memory boxes, distributed-memory clusters, and supercomputers are examples of this.

LAMMPS keeps track of adjacent particles via neighbor lists. The lists are tuned for systems with particles that repel each other over short distances, so that the local particle density never grows too large.[40] This differs from approaches used to represent plasma or gravitational bodies.

3.2.4. Molecular Dynamics Simulation Details

The MD simulation is ran based on LAMMPS(Large-scale Atomic/Molecular Massively Parallel Simulator). Periodic boundaries conditions is set for every simulation in all directions. The velocity-Verlet algorithm is used to integrate the equations of motion with a time step of 1 fs. For the two-site H_2 and H_2O force fields, the bond lengths and the angle in H_2O are fixed using the SHAKE algorithm in LAMMPS. Intermolecular interactions are described using just Lennard-Jones (LJ) and Coulombic potentials. The LJ and electrostatic cutoff radii are determined using the original H_2 and H_2O force fields. To compute the long-range electrostatic energy, the particle-particle particle-mesh (PPPM) technique with a relative error of 105 is utilized. Energy and pressure are subjected to analytic tail corrections. For interactions between dissimilar species, the Lorentz-Berthelot combining rules are applied.. All initial configurations are created using PACKMOL software by fftool. The Nosé−Hoover thermostate is used to control the temperature and the pressure of the system.

Initially, the system is energy minimized, consequently, equilibration runs are performed in the NpT and NVT ensembles for 1−2 ns, and finally the properties are sampled from production runs in the NVE ensemble. The simulation time for the NVE ensemble is 10ns for each running. At this running time, properly converged mean-squared-displacements (MSD) for the computation of the transport coefficients can be achieved.
In all the MD simulations, 700 water molecules and 2 hydrogen molecules are used.

3.3. Main equations

OCTP(On-the-fly computation of transport properties) plugin[5] in LAMMPS is used to calculate the self- and intradiffusivities, as well as shear viscosities.

In a single simulation, OCTP computes the self- and Maxwell-Stefan diffusivity, bulk and shear viscosity, and thermal conductivity of pure fluids and mixtures. It is a tool for calculating fluid transport parameters on the fly utilizing Einstein relations in conjunction with the Order-n algorithm in LAMMPS for efficient sampling of dynamic variables. In the OCTP plugin, the calculation is based on the Einstein relation, as shown in 2.3 and 2.6 in the above chapter.

Verlet algorithm
Verlet algorithm is a numerical method for solving Newton's equations of motion, widely used in molecular dynamics simulations and video games. The advantage of the Verlet algorithm is that it is numerically stable much more stable than the simple Euler method, and maintains the properties of time reversibility and volume conservation of phase space volume elements in physical systems.

The problem to be solved by the Verlet algorithm is that, given the position r and momentum p (velocity v) of the particle at time t, the position $r(t + dt)$ and momentum $p(t + dt)$.

Order-n algorithm
At various sampling frequencies, the order-n method samples time-correlation functions or MSDs[41]. For each sample frequency, many blocks (buffers) are formed. Based on the varied sampling frequencies, it is determined if a buffer has to be updated for each simulation timestep. To compute the time-correlation function/MSD, the oldest entry in the buffer is utilized as the origin. The calculated value is added to an array, which will be used to calculate the ensemble-averaged MSD. The buffer's oldest element is removed, and all other items are relocated one step to make room for the newest system property, and this method is repeated.

Finite size effect
In simulations, finite size effects are common. Such effects can be caused by a variety of factors, including a finite number of particles in a finite system, a finite simulation box when using periodic boundary conditions, a finite basis set in quantum chemistry, a finite time step or grid spacing in algorithms, and incomplete sampling of phase space due to finite computational time.

The practical implications of such finiteness are numerous, with dramatic implications on computed properties and the (lack of) ability to compare simulation results with experiments, which correspond

in principle to a ”infinite limit”: thermodynamic limit (N), continuous limit ($\Delta t \rightarrow 0, \Delta x \rightarrow 0$), and so on. These consequences are often seen as a nuisance, and effective strategies for correcting them are created. In this work, all diffusivities are corrected for finite-size effects using the Yeh−Hummer equation[42].

$$D_i^{\infty} = D_i + \frac{k_B T \xi}{6\pi\eta L} \tag{3.4}$$

in which k_B is the Boltzmann constant, η is the shear viscosity of the system computed from simulation, and $D_i$is the self diffusivity in the thermodynamic limit. η computed in the simulation does not show finite-size effects. ξ is a constant which depends on the shape of the simulation box (for a cubic simulation box, ξ = 2.837297). And this correction function is well validated by a lot of works.[42][43]

4

Results and Discussion

All of the simulation findings are discussed in this chapter. The reason of choosing the type of water model and hydrogen model are discussed at first. Then the simulation is carried out with different ions forcefields. Following the previous discussions and studies, a large production using the given models and force fields is built with varying morality, temperature, and pressures which related to the underground hydrogen storage applications.

Previous studies have shown that the TIP4P/2005 force field can accurately capture the transport properties of pure H_2O and aqueous solutions for a broad range of conditions. When it came to the shear viscosity at ambient conditions, The performance of TIP4P/2005 is excellent, that of SPC/E is more or less acceptable[44].

For the selection of the hydrogen model, from the study of Tsimpanogiannis et al.[22], the self diffusion coefficient results of different hydrogen forcefields are presented and discussed, which shows the three-site models perform significantly better than the rest. The Silvera Goldman[33] force field has the best accuracy (absolute average variation from experimental data equal to 4.6 %), followed by the Marx[34] force field (deviation of 4.8%). Among the single and two-site force fields, the Buch38 force field has an accuracy equivalent to the three-site models (6.7%). For the majority of temperatures and pressures, the force fields exhibit mutual consistency, with Silver-Goldman[33] being the most accurate and Cracknell[32] being the least accurate.

But when it comes to the calculation of the gas in the aqueous solutions, the three-site model of hydrogen must be calculated with fix rigid command but not suitable for the SHAKE algorithm while SHAKE algorithm can run three times faster than the rigid one. Because of the limitation of the rigid LAMMPS command, each rigid body must have two or more atoms. An atom can belong to at most one rigid body. The ions(Na^+, Cl^-) in the solutions must be created with a dummy site in order to run the simulation. Single-site hydrogen model is therefore be chosen as the suitable hydrogen model for the following simulations.

4.1. Ions forcefield Measurement

As mentioned in the above Chapter 3, there are two kinds of force fields developed by Vegas et al. The complete information for these two models can be found in table 3.7 and table 3.8. To compare these two models more effectively, simulations based on these forcefields are run under the following conditions: temperature equals 298 K, pressure equals 1 bar, and the Vrabec model of hydrogen is used. For each certain condition, 5 simulations based on different initial random seeds took place for the statistics to reduces the calculation error. The simulations are used to test the NaCl solution from 1 mol/kg to 8 mol/kg in order to better compare the results.

4.1.1. Density

The density output is depicted in the figure 4.1. The figure shows that the computed results under the two force fields correspond well with the density fitting of the literature data, indicating that both force fields perform well when estimating the density of the NaCl system.

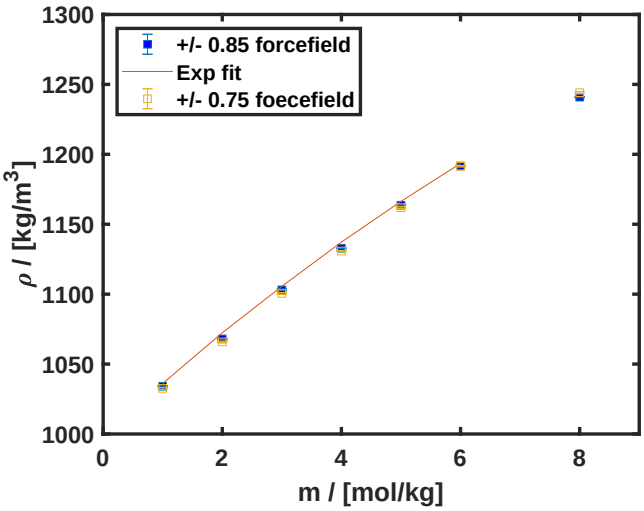

Figure 4.1: The results of the density calculation for two different ions forcefields, fit of experimental data taken from ref [45]

4.1.2. Shear viscosity

The outcome of the computation of the shear viscosity of two distinct ions forcefields is shown below in figure 4.2. Both the 0.75 charger and 0.85 charger forcefields suit the experimental data well for the low concentrations of NaCl solutions. However, when it comes to the high molalities of the whole system, the 0.85 forcefield values are significantly higher than the experimental data, whilst the other one exhibits complete agreement. When estimating the shear viscosity of the NaCl system, the 0.75 charger forcefield is clearly superior, especially at large concentrations.

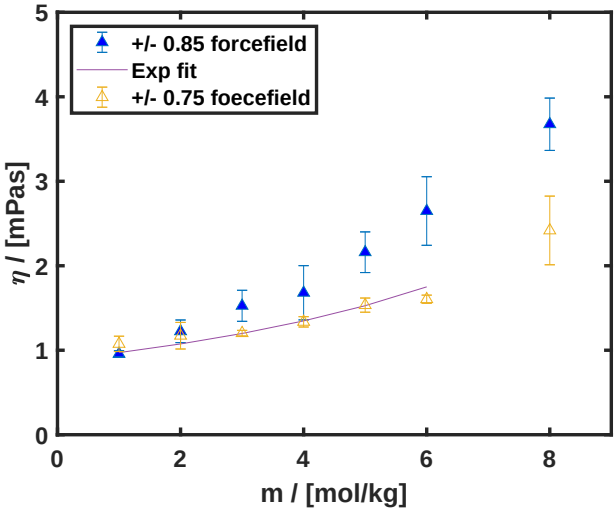

Figure 4.2: The results of the viscosity calculation for two different ions forcefields(0.85 Madrid forcefield and 0.75 Madrid forcefield), fit of experimental data taken from ref [45]

4.1.3. Diffusion coefficient

The outcome of the computation of the diffusion coefficient of water in the solutions of two distinct ions forcefields is shown below in figure 4.3. Although because of the lack of the experimental data

the properties cannot be compared with the realistic ones, the agreement of the two lines shows that both the forcefield have likely results when it comes to the low concentrations. When it comes to high molalities, the 0.75 forcefields has a higher output as the 0.85 forcefield. In this case, when it comes to the massive calculation of the diffusion coefficient, both forcefield are needed to be considered.

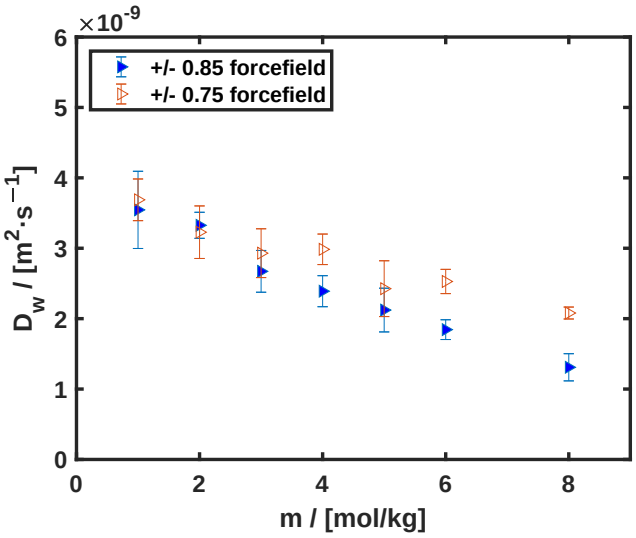

Figure 4.3: The results of the self diffusion coefficient of water in NaCl solutions using two different ions forcefields, the x-axics line shows the different molalities of the NaCl solutions

4.2. Simulation conditions

Based on the above discussion about the selection of the forcefields, TIP4P/2005 water model, Vrabec hydrogen model are used in the following simulations. For low concentrations 0.85 charger ions forcefield is used, and when it comes to the high concentrations, 0.75 charger ions forcefield is also calculated for the comparison. Also, not all pressures are possible in combination with each temperature, because water will not be a liquid in all cases. For example for T=523.15 K, simulations for 1 and 10 bar are not considered, since on the NIST website that water will be a gas at that combined condition. It is same when temperature equals to 723K, in this case only 400bar and 1000bar are possible for a liquid state of the whole system. The detailed simulation conditions which are related to the underground hydrogen storage are shown in the following table 4.1 and table 4.2.

For each condition, 5 simulations with different initial random seed are run for the statistics analysis.

Table 4.1: Initial setup for all the simulations details: 0.85 ions forcefield

Simulation details: Initial setup				
Temperature[K]	298	343	523	723
Molality[mol/kg]	1, 3, 5, 8	1, 3, 5, 8	1, 3, 5, 8	1, 3, 5, 8
Pressure[bar]	1,10,100,400,1000	1,10,100,400,1000	100, 400, 1000	400, 1000

Table 4.2: Initial setup for all the simulations details: 0.75 ions forcefield

Simulation details: Initial setup				
Temperature[K]	298	343	523	723
Molality[mol/kg]	5, 8	5, 8	5, 8	5, 8
Pressure[bar]	1,10,100,400,1000	1,10,100,400,1000	100, 400, 1000	400, 1000

4.3. Density

In this section, the density results of the simulations in different temperature and pressures for various molalities are presented. The simulation results are compared with the literature data created by Laliberté et al.[45] and ref [46].

4.3.1. Molality Effect

The following figures show the results when temperature is 298K, 343K, 523K and 723K versus different molalities. They show the results of the density calculation. From these figures it is clear to see that with high molalities the density of the whole system is obviously increase. And the calculated result have a great agreement with the experimental data at 298K and 343K. For high temperature and high pressures, the experimental data can hardly be found.

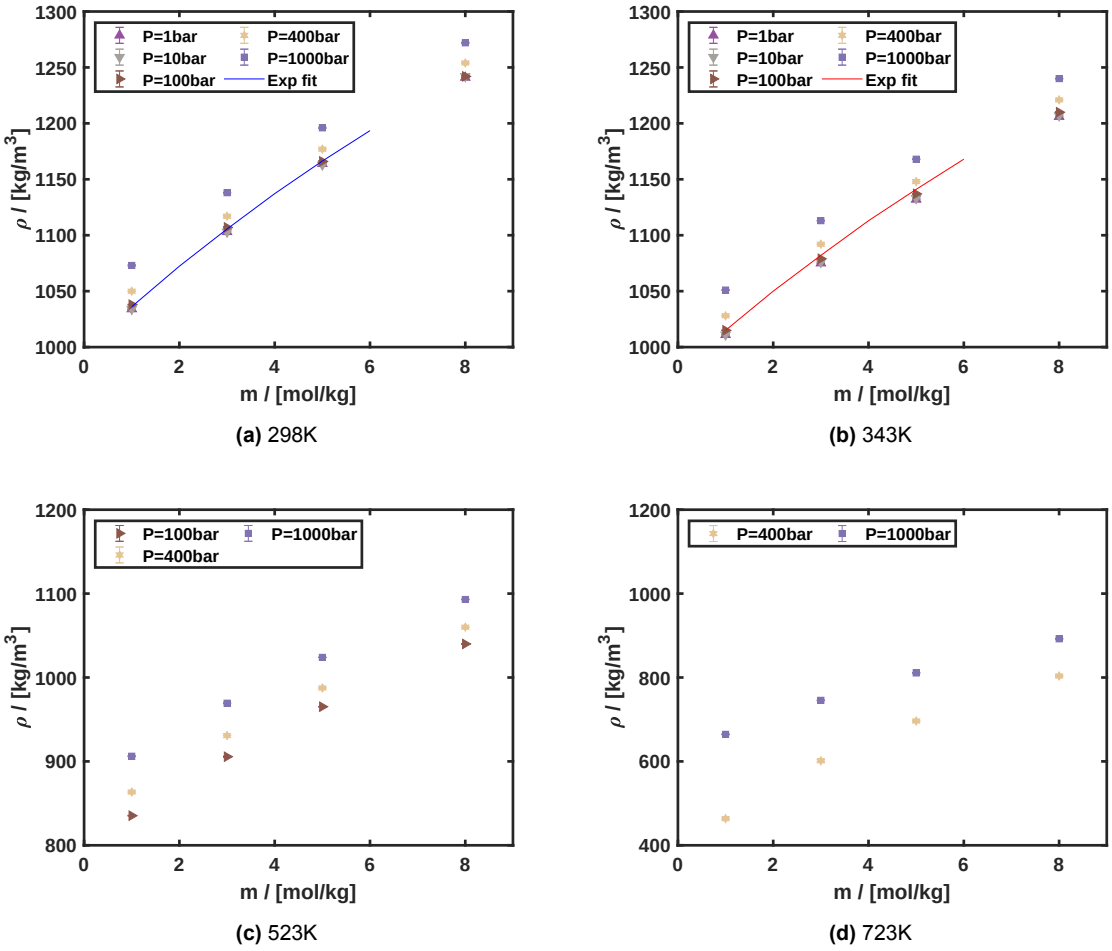

(a) 298K **(b)** 343K

(c) 523K **(d)** 723K

Figure 4.4: Density calculation results using 0.85 Mardrid forcefield at (a)298K, (b)343K, (c)523K, (d)723K, fit of experimental data in (a) taken from ref [45], fit of experimental data in (b) taken from ref [46].

4.3.2. Pressure Effect

From the figure of 298K and 343K which shows above, it can be seen that when the pressure value fluctuates in the range of 1-100 bar, the simulated density calculation results hardly change and match the experimental values from the literature very well. When the pressure reaches 1000bar, the results of the density is higher than the low pressure conditions.

When it comes to the same concentration at the same pressure for different temperatures, with higher temperature, the density of the whole system became lower. The following graph 4.5 describes the density changes when the pressure varies under the same temperature. The flat line indicates that the

different pressure for the same temperature does not impacts a lot when it comes to the calculation of the density of the system.

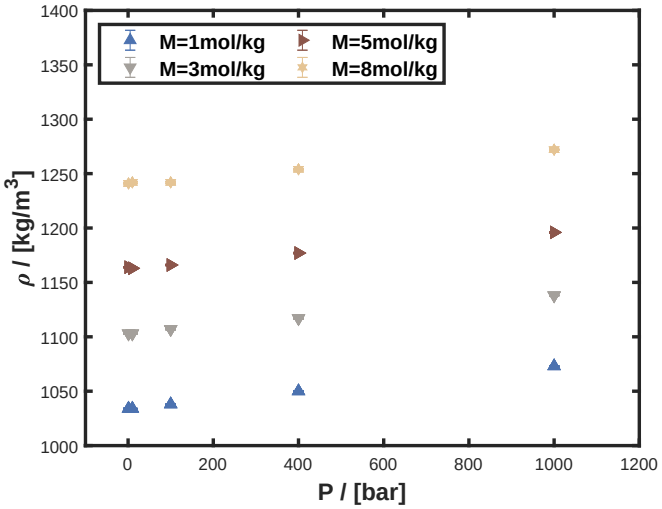

Figure 4.5: The results of the density calculation for different molalities of NaCl solution at 298K under different Pressures

4.3.3. Temperature Effect

Take the following condition as an example, when the molality of NaCl solution are the same, and pressure equals to 400bar, the results of the calculation of the density is shown in the following table:

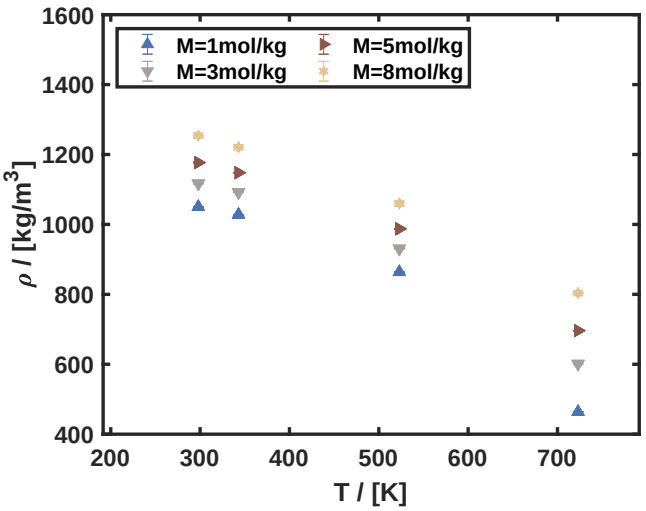

Figure 4.6: The results of the de nsity calculation for different molalities of NaCl solution at 400bar under different temperatures

It is obvious that when the temperature rises, the density of the whole system falls when all the simulation runs at the same pressure. When the temperature rises, the volume expands due to thermal expansion, and the density of the entire system falls.

4.4. Shear viscosity

In this section, the viscosity results of the simulations in different temperature and pressures for various molalities are presented. The final results combined two different ions forcefields. For low concentrations, 0.85 ions forcefield is used while for molalities as 5 mol/kg and 8 mol/kg, 0.75 ions forcefield is

used, following the discussion in the previous sections. The simulation results are compared with the literature data created by Laliberté et al.[45] and ref [47].

4.4.1. Molality Effect

The following figures show the results of the shear viscosity calculation at all the selected temperatures.

From the figures it is clear that the shear viscosity of the NaCl solutions will increase as the molality of NaCl increase. Combining the two ions forcefields help with the fitting with the experimental data at high molality when it comes to 5 mol/kg solutions.

For the simulations which is taken with higher temperature as 523K and 723K, the following figures show the results of the shear viscosity calculation. For these high temperature and high pressures, the experimental data of the shear viscosity of these solutions can hardly be found.

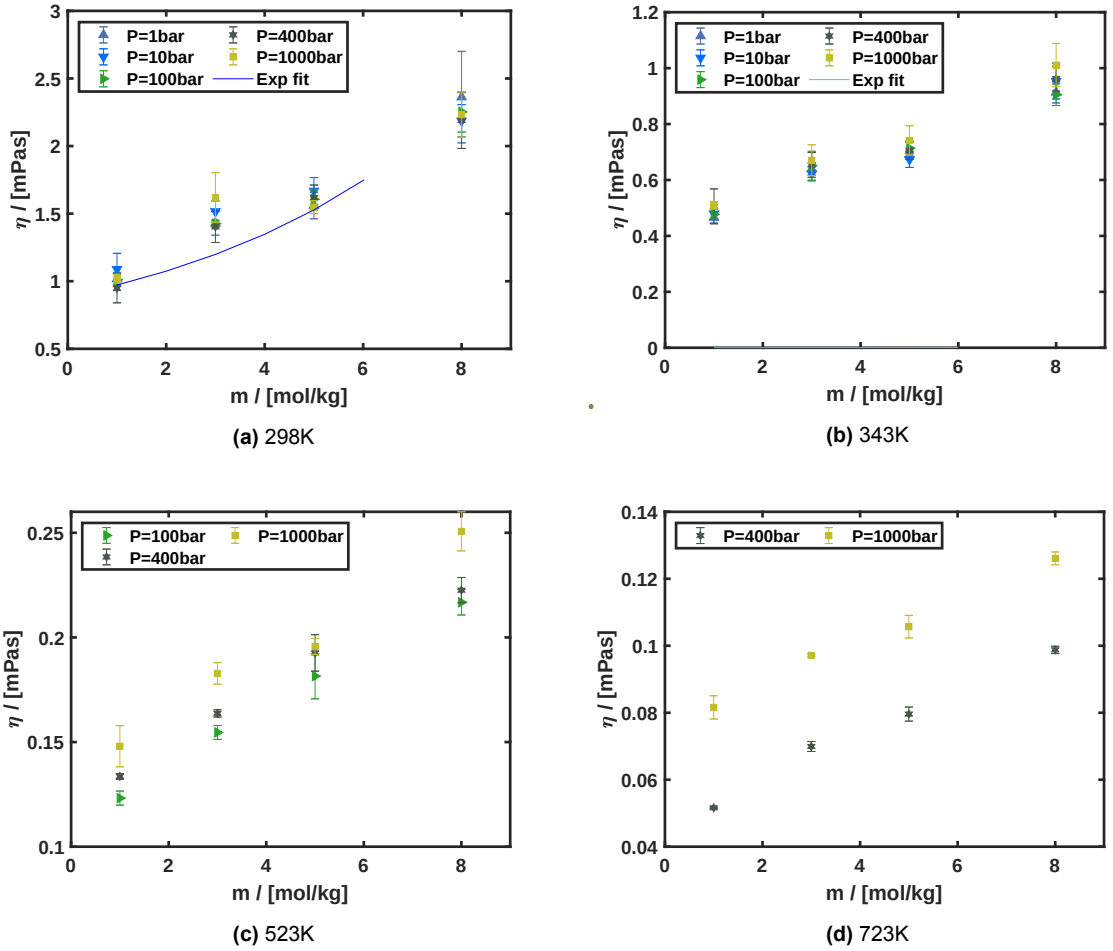

Figure 4.7: Shear viscosity calculation results using 0.85 Mardrid forcefield at (a)298K, (b)343K, (c)523K, (d)723K, fit of experimental data in (a) taken from ref [45], fit of experimental data in (b) taken from ref [47]

4.4.2. Pressure Effect

Take the following condition as an example, when the molality of NaCl solution are the same, and temperature equals to 298K, the following figure shows the shear viscosity changes with the pressure. Although from the figure 4.8 in the previous subsection, it shows that with higher pressures at the same temperature, the shear viscosity becomes higher, the changes is not that significant. Basically the changes which is caused by the pressure conditions has a small impact on the final results.

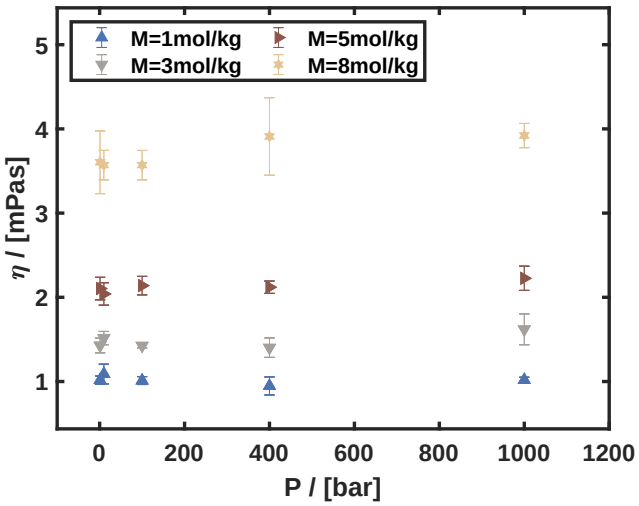

Figure 4.8: The results of the shear viscosity calculation for different molalities of NaCl solution at 298K under different Pressures

As what is discussed before, the result of different forcefield calculation varies and the 0.75 forcefield shows better agreement when it comes to the high molality solutions for the viscosity calculation. Following is the figure which combined the results of both 0.75 forcefield and 0.85 forcefield when it comes to high molalities. From the figure it is obvious the result of 0.85 forcefield when it comes to 8 mol/kg is extremely high compared to the 0.75 forcefield calculation results, while the result of 0.75 forcefield is more acceptable. But what is the same for all the results is that the pressure effect is quite minor.

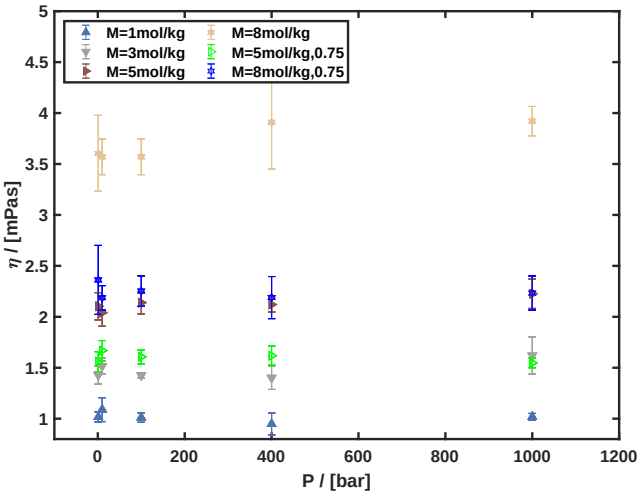

Figure 4.9: The results of the shear viscosity calculation for different molalities of NaCl solution at 298K under different Pressures, combining the results of 0.75 forcefield and 0.85 forcefield.

4.4.3. Temperature Effect

Take the following condition as an example, when the molality of NaCl solution are the same, and pressure equals to 400bar, the results of the calculation of the shear viscosity is shown in the following figure 4.10:

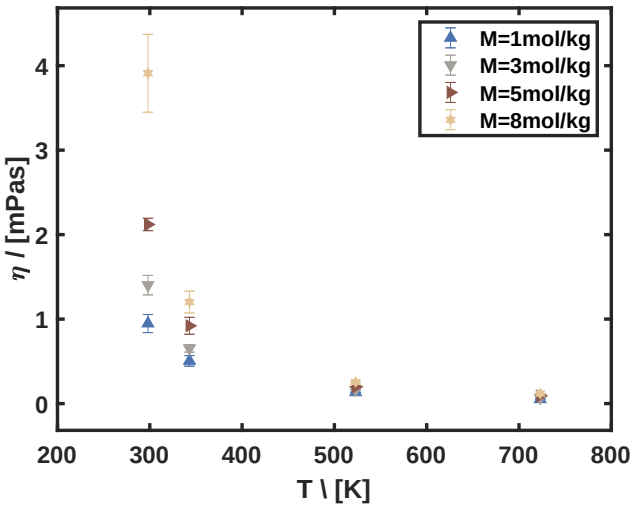

Figure 4.10: The results of the viscosity calculation for different molalities of NaCl solution at 400bar under different temperatures

The trend of the figure clearly shows that when it comes to the same system under the same pressure, when the temperature increase the shear viscosity of the system decrease. That is because the liquid's viscosity is caused by molecular attraction. As the temperature rises, the distance between molecules grows, so that the molecular attraction decreases, and internal friction becomes weaker, resulting in a decrease in viscosity.

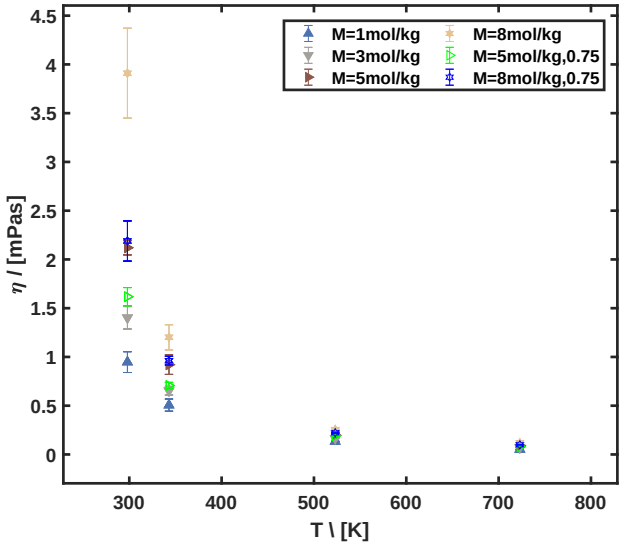

Figure 4.11: The results of the viscosity calculation for different molalities of NaCl solution at 400bar under different temperatures, combining the results of 0.75 forcefield and 0.85 forcefield.

The results which are shown in figure 4.11 shows the decrease trend of viscosity when the temperature arise and also give the clear comparison between the 0.75 forcefield and 0.85 forcefield calculation. With 0.75 forcefield, the shear viscosity in high molalities show lower results which is the same trend as what has been discussed before.

4.5. Self diffusion coefficient

4.5.1. Self diffusion coefficient of water

The following figures show the calculation results of self diffusion coefficient of water in NaCl solutions under different temperatures, pressures and molalities of NaCl solutions.

NaCl molalities Effect

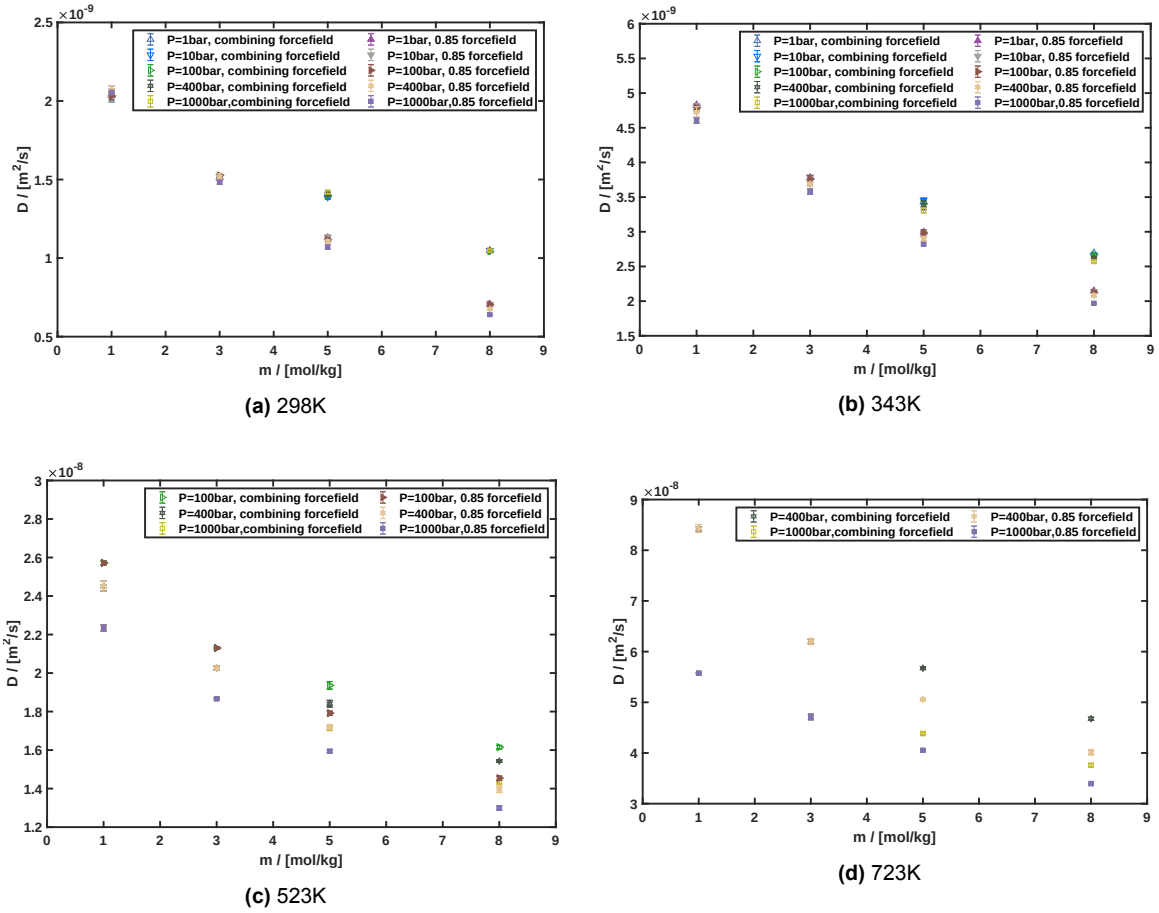

(a) 298K **(b)** 343K

(c) 523K **(d)** 723K

Figure 4.12: Diffusion coefficient of water in the different molalities of NaCl solutions using 0.85 Mardrid forcefield and combining forcefield at (a)298K, (b)343K, (c)523K, (d)723K

From the figures above it is clear that in the different molalties of the NaCl solutions, with the increase number of the other ions in the system, the self diffusion coefficient of the solvent decrease. The 0.75 ions forcefields shows higher diffusion coefficient results compared to the 0.85 forcefield.

Pressure Effect

The following figure 4.13 shows the example condition when taking temperature as 298K with different molalities of the NaCl solutions. The flat linear shows that the self diffusion coefficient of water at the same temperature will not be impacted by the changes of the pressure of the whole system.

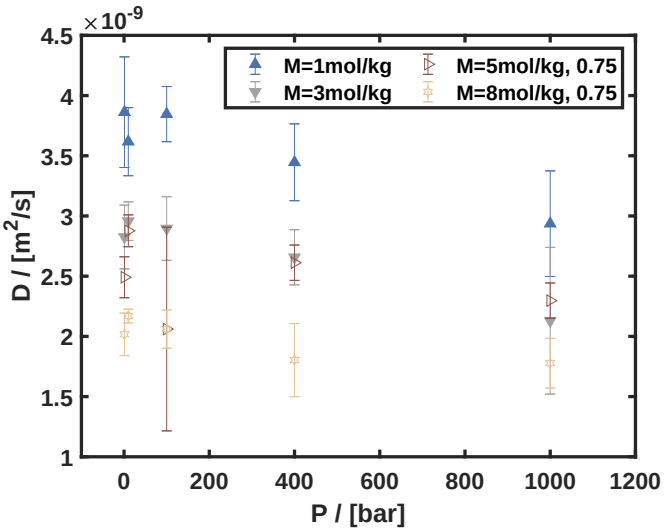

Figure 4.13: The results of the self-diffusion coefficient of water in different molalities of NaCl solution at 298K under different Pressures, for 1 mol/kg and 3mol/kg solutions, 0.85 forcefield is used while for 5 mol/kg and 8mol/kg, 0.75 forcefield is used.

Temperature Effect

Take the following condition as an example, when the molality of NaCl solution are the same, and pressure equals to 400bar, the results of the calculation of the self diffusion coefficient of water are shown in the following figure 4.14:

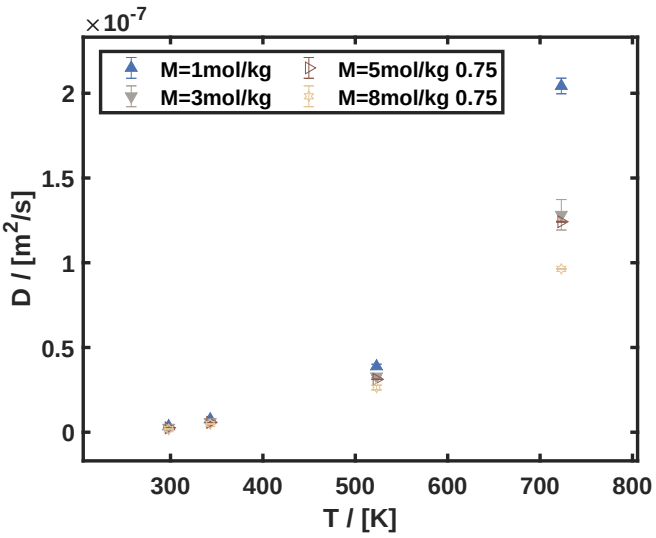

Figure 4.14: The results of the self-diffusion coefficient of water in different molalities of NaCl solution at 298K under different Pressures, for 1 mol/kg and 3mol/kg solutions, 0.85 forcefield is used while for 5 mol/kg and 8mol/kg, 0.75 forcefield is used.

The trend of the figure clearly shows that when it comes to the same system under the same pressure, when the temperature increase the self diffusion coefficient of water in the system increase. With higher temperature, the kinetic energy of the whole system goes higher, the higher self-diffusion coefficient therefore exists.

4.5.2. Self diffusion coefficient of ions

The following figures show the calculation results of self diffusion coefficient of ions in NaCl solutions under different temperatures, pressures and molalities of NaCl solutions.

NaCl molalities Effect

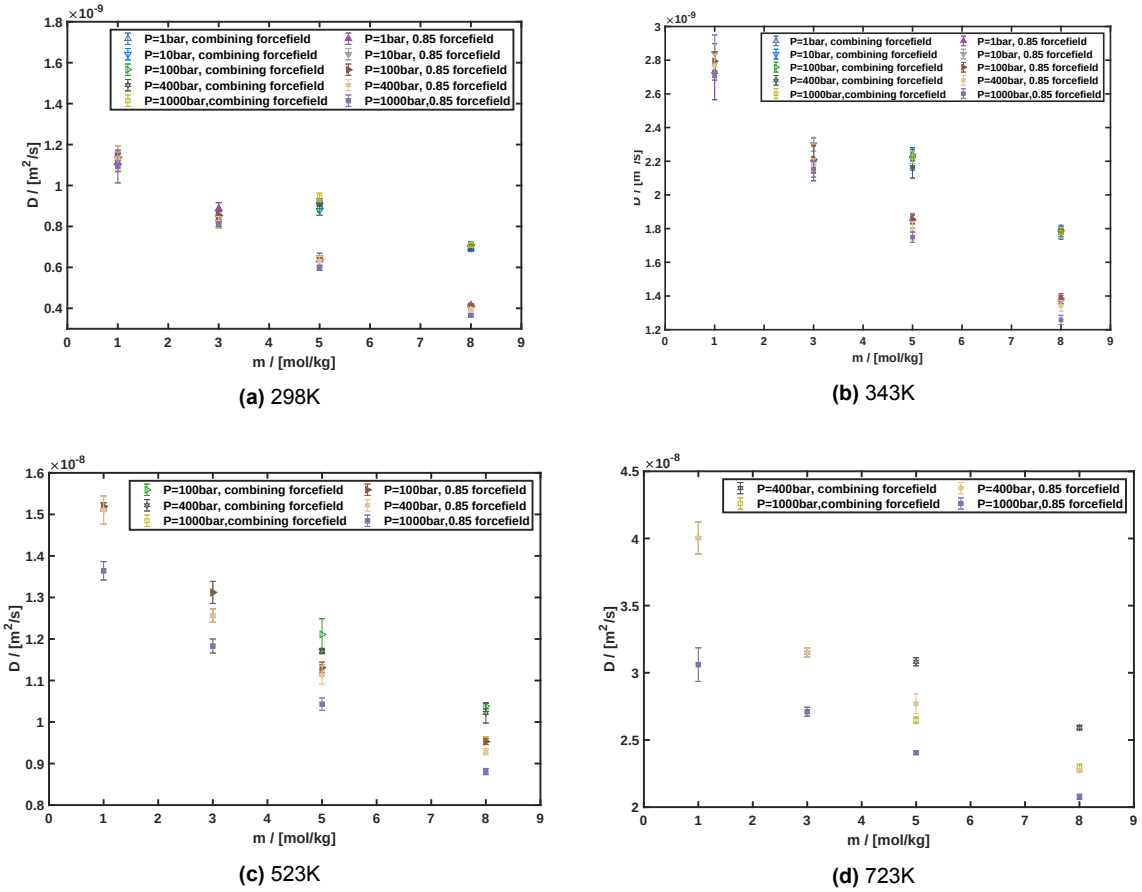

Figure 4.15: Diffusion coefficient of Na^+ in the different molalities of NaCl solutions using 0.85 Mardrid forcefield and combining forcefield at (a)298K, (b)343K, (c)523K, (d)723K

From the figure 4.15 and figure 4.16, it is clear that in the different molalties of the NaCl solutions, with the increase number of the ions in the system, the self diffusion coefficient of the both ions decrease. Both the cation and anion shows the same trend when the molalities go up. Also, the 0.75 ions forcefields shows higher diffusion coefficient results compared to the 0.85 forcefield.

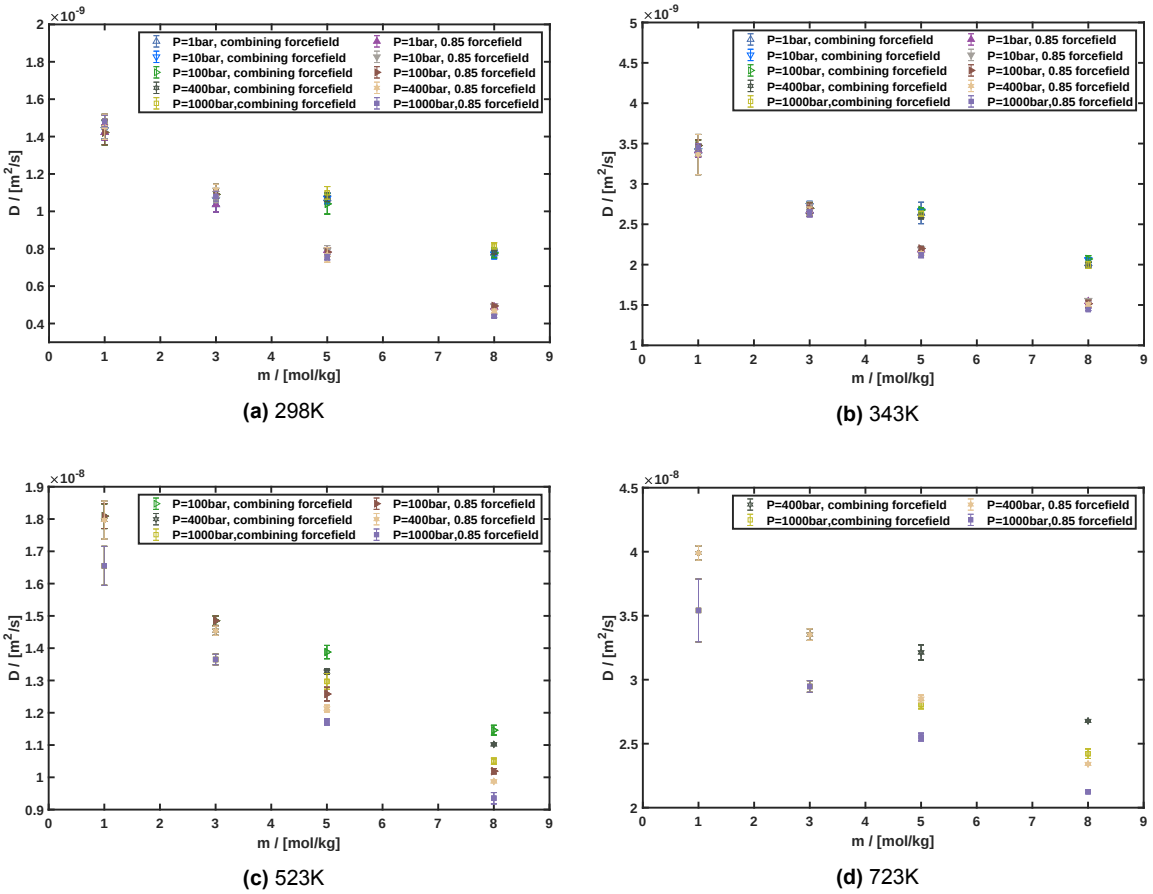

(a) 298K **(b)** 343K

(c) 523K **(d)** 723K

Figure 4.16: Diffusion coefficient of Cl^- in the different molalities of NaCl solutions using 0.85 Mardrid forcefield and combining forcefield at (a)298K, (b)343K, (c)523K, (d)723K

Pressure Effect

The following table 4.3 gives the example of the results of the calculation of the self diffusion coefficient of water for the same molality at 298K for different pressures.

From the example results in the table 4.3, the comparison of the D of Na^+ and Cl^- is obvious that the results of the Cl^- is higher, which means with larger molar mass, the self diffusion coefficient will be higher.

The following figure 4.17 and figure 4.18 shows the example condition when taking temperature as 298K with different molalities of the NaCl solutions. The flat linear shows that the self diffusion coefficient of both ions at the same temperature will not be impacted by the changes of the pressure of the whole system.

Table 4.3: Example: Self-diffusion coefficient of ions in 1 mol/kg NaCl solution at 298K under different pressures

P [bar]	$D_{Na^+}[10^{-9}m^2/s]$	$\sigma_{D\,Na^+}[10^{-9}m^2/s]$	$D_{Cl^-}[10^{-9}m^2/s]$	$\sigma_{D\,Cl^-}[10^{-9}m^2/s]$
1	1.112	0.04	1.422	0.04
10	1.131	0.03	1.437	0.05
100	1.138	0.01	1.422	0.07
400	1.133	0.06	1.452	0.07
1000	1.093	0.08	1.483	0.03

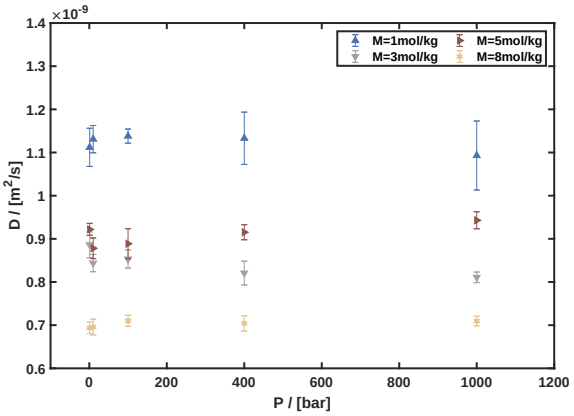

Figure 4.17: The results of the self-diffusion coefficient calculation for different molalities of Na^+ at 298K under different Pressures, for 1 mol/kg and 3mol/kg solutions, 0.85 forcefield is used while for 5 mol/kg and 8mol/kg, 0.75 forcefield is used.

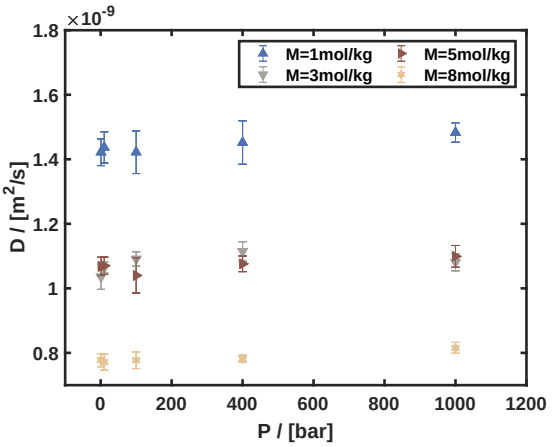

Figure 4.18: The results of the self-diffusion coefficient calculation for different molalities of Cl^- at 298K under different Pressures, for 1 mol/kg and 3mol/kg solutions, 0.85 forcefield is used while for 5 mol/kg and 8mol/kg, 0.75 forcefield is used.

Temperature Effect

Take the following condition as an example, when the molality of NaCl solution are the same, and pressure equals to 400 bar, the results of the calculation of the self diffusion coefficient of ions are shown in the following table 4.4 and figures:

Table 4.4: Example: Self-diffusion coefficient of Na^+ and Cl^- in 1 mol/kg NaCl solution under 400bar at different temperatures

T[K]	$D_{Na^+}[10^{-9}m^2/s]$	$\sigma_{D\,Na^+}[10^{-9}m^2/s]$	$D_{Cl^-}[10^{-9}m^2/s]$	$\sigma_{D\,Cl^-}[10^{-9}m^2/s]$
298	1.13	0.06	1.452	0.07
343	2.77	0.06	3.364	0.25
523	15.11	0.34	17.97	0.59
723	40.03	1.18	39.90	0.56

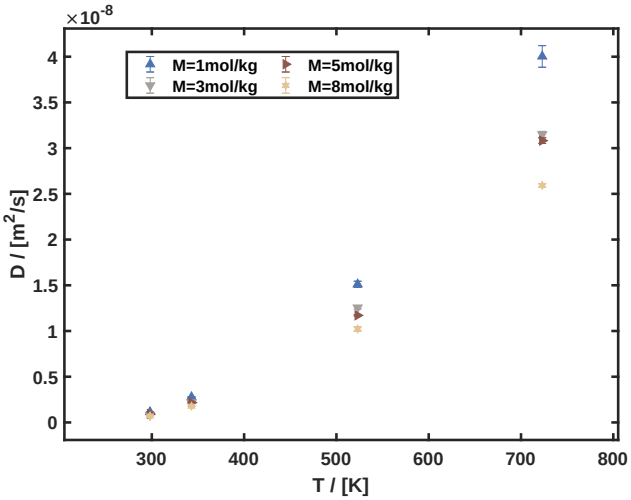

Figure 4.19: The results of the self-diffusion coefficient calculation for different molalities of Na^+ at 298K under different Pressures, for 1 mol/kg and 3mol/kg solutions, 0.85 forcefield is used while for 5 mol/kg and 8mol/kg, 0.75 forcefield is used.

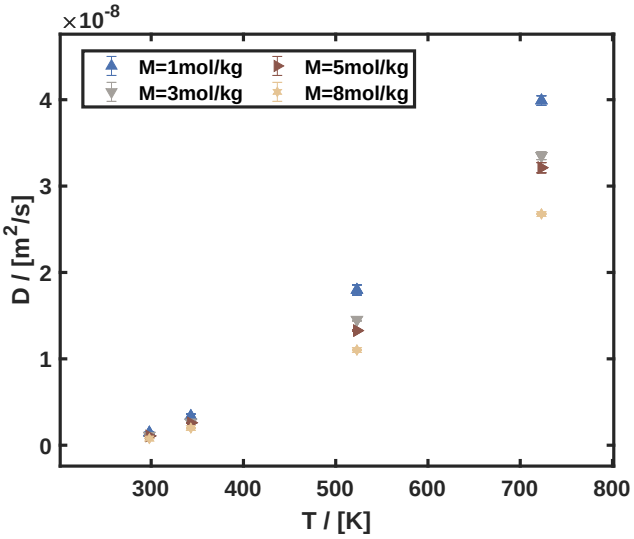

Figure 4.20: The results of the self-diffusion coefficient calculation for different molalities of Cl^- at 298K under different Pressures, for 1 mol/kg and 3mol/kg solutions, 0.85 forcefield is used while for 5 mol/kg and 8mol/kg, 0.75 forcefield is used.

The trend of the figure clearly shows that when it comes to the same system under the same pressure, when the temperature increase the self diffusion coefficient of water in the system increase. With higher temperature, the kinetic energy of the whole system goes higher, the higher self-diffusion coefficient therefore exists.

4.5.3. Self diffusion coefficient of hydrogen

With 2 molecules of hydrogen in the various molalities of sodium chloride solution system, the self diffusion coefficient is calculated under different pressures and temperatures. How the self diffusion coefficient changes with solution molalities, pressures and temperatures will show in the following sub-sections.

NaCl molalities Effect

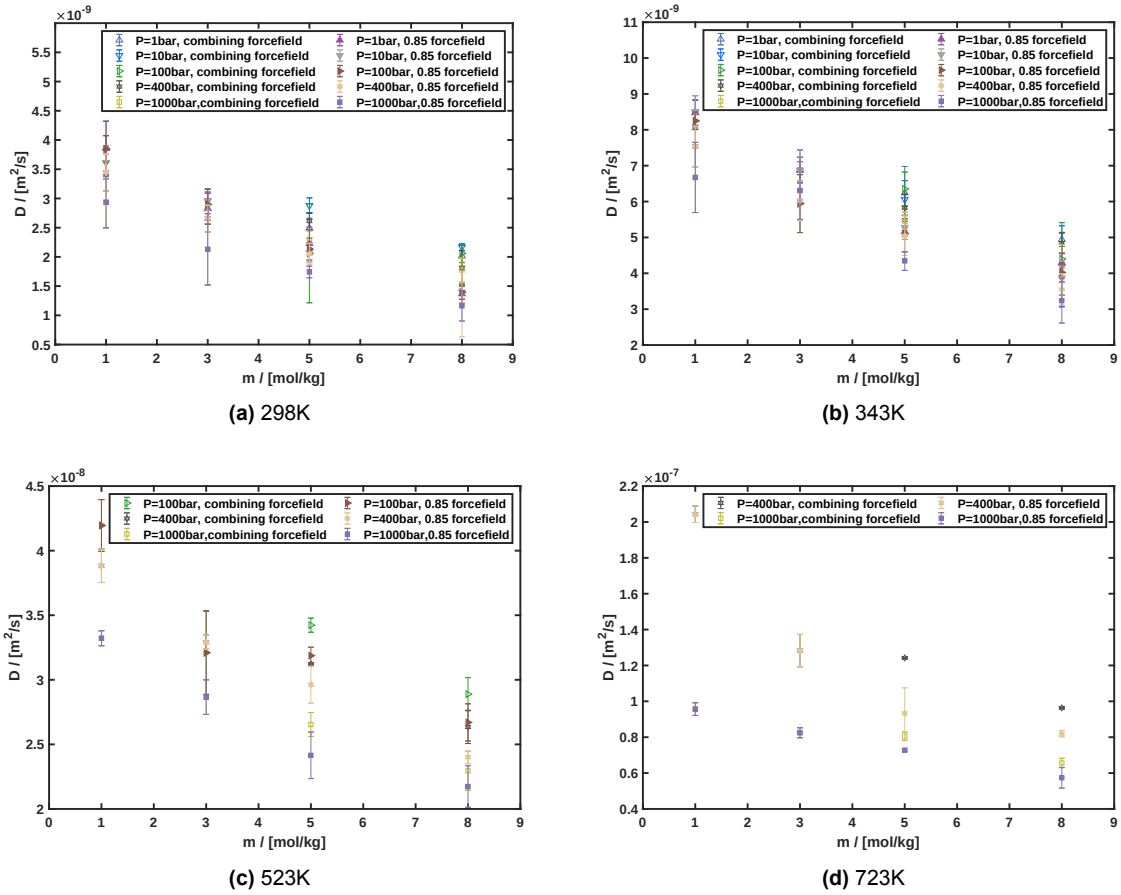

Figure 4.21: Diffusion coefficient of H_2 in the different molalities of NaCl solutions using 0.85 Mardrid forcefield and combining forcefield at (a)298K, (b)343K, (c)523K, (d)723K

From the figures above it is clear that in the different molalties of the NaCl solutions, with the increase number of the other ions in the system, the self diffusion coefficient of the hydrogen decrease. The 0.75 ions forcefields shows higher diffusion coefficient results compared to the 0.85 forcefield.

Pressure Effect

Figure 4.22 shows the relation of self diffusion coefficient and pressures. And table 4.5 gives the example results of condition while the NaCl solution is 1 mol/kg and temperature is 298K. The line is relatively flat in the high molalities of the NaCl solution systems and the fluctuation is not that obvious. Buw when it comes to the relatively high pressures, the self diffusion coefficient is lower that the low ones.

Table 4.5: Example: Self-diffusion coefficient of hydrogen in 1 mol/kg NaCl solution at 298K under different pressures

Pressure[bar]	1	10	100	400	1000
D_{H}[10^{-9}m^2/s]	3.86	3.62	3.86	3.44	2.94
$\sigma_{D\mathrm{H}}$[10^{-9}m^2/s]	0.46	0.28	0.23	0.32	0.44

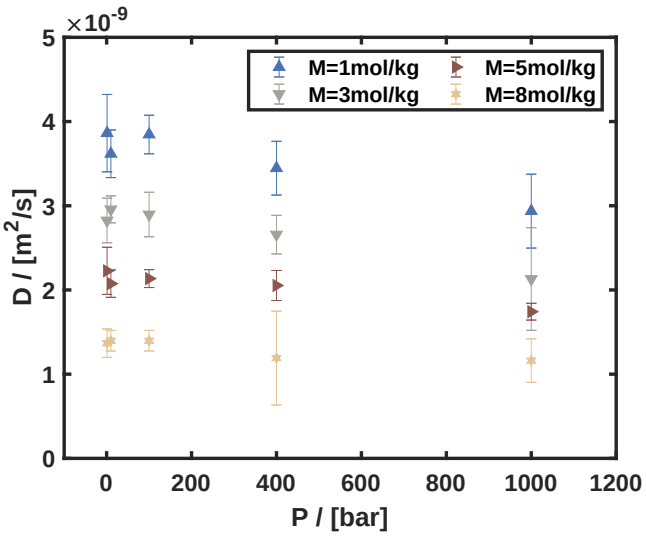

Figure 4.22: The results of the self-diffusion coefficient calculation for different molalities of hydrogen at 298K under different Pressures, for 1 mol/kg and 3mol/kg solutions, 0.85 forcefield is used while for 5 mol/kg and 8mol/kg, 0.75 forcefield is used.

Temperature Effect

Take the following condition as an example, when the molality of NaCl solution are the same, and pressure equals to 400bar, the results of the calculation of the self diffusion coefficient of water are shown in the following figure 4.23. It can be seen from both the table and the figure that with the temperature increase, the self coefficient of the hydrogen also increase. For the low concentrations of NaCl solution systems, the rise is more significant than the higher ones.

Table 4.6: Example: Self-diffusion coefficient of hydrogen in 1 mol/kg NaCl solution under 400 bar for different temperatures

Temperature[K]	298	343	523	723
$D_{\mathrm{H}}[10^{-9}\mathrm{m}^2/\mathrm{s}]$	3.45	7.54	38.83	204.30
$\sigma_{D\mathrm{H}}[10^{-9}\mathrm{m}^2/\mathrm{s}]$	0.32	0.57	1.30	4.60

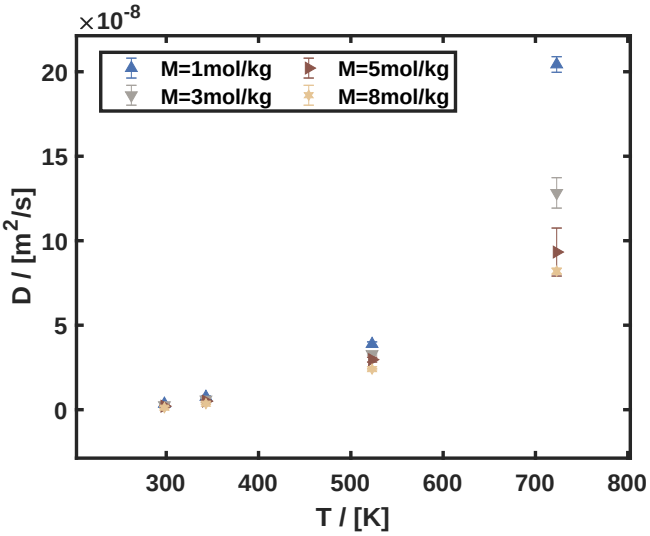

Figure 4.23: The results of the self-diffusion coefficient calculation for different molalities of hydrogen at 400bar for different temperatures, for 1 mol/kg and 3mol/kg solutions, 0.85 forcefield is used while for 5 mol/kg and 8mol/kg, 0.75 forcefield is used.

4.6. D_{H_2} in pure water and NaCl solutions systems

The self diffusion coefficient of hydrogen are also discussed in this section with the comparison between pure water system and the aqueous solutions.

4.6.1. Pressure Effect

In this subsection, the diffusion coefficient of hydrogen at 298K in pure water and 1 mol/kg NaCl solutions are compared.

From the table 4.7 and figure 4.24, it can be seen that the diffusion coefficient of hydrogen does not change a lot as the pressure goes higher in these two different systems, while the coefficient is higher in pure water than in the aqueous solutions.

Table 4.7: Example: Self diffusion coefficient of hydrogen in pure water and 1 mol/kg NaCl solutions at 298K under different pressures

Pressure[bar]	D_{H_w}[10^{-9}m^2/s]	$\sigma_{D\mathrm{H}_w}$[10^{-9}m^2/s]	D_{H}[10^{-9}m^2/s]	$\sigma_{D\mathrm{H}}$[10^{-9}m^2/s]
1	4.43	0.19	3.86	0.46
10	4.49	0.33	3.62	0.28
100	4.60	0.41	3.85	0.23
400	3.91	0.30	3.45	0.32
1000	4.08	0.07	2.94	0.44

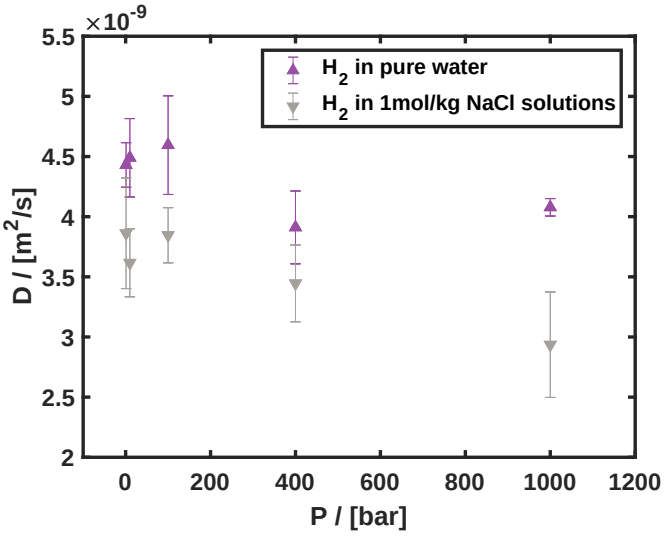

Figure 4.24: The results of the self-diffusion coefficient calculation for hydrogen at 298K in pure water and NaCl solutions under different Pressures, 0.85 Madrid forcefield is used for the NaCl solutions

4.6.2. Temperature Effect

From the following table 4.8 and the figure 4.25, the trend of the self diffusion coefficient with the changes of the temperature is obvious. With the increase of the temperature, the diffusion coefficient of hydrogen becomes higher.

Table 4.8: Example: Self diffusion coefficient of hydrogen in pure water and 1 mol/kg NaCl solutions under 400bar at different temperatures

T [K]	D_{H_w}[10^{-9}m^2/s]	$\sigma_{D\mathrm{H}_w}$[10^{-9}m^2/s]	D_{H}[10^{-9}m^2/s]	$\sigma_{D\mathrm{H}}$[10^{-9}m^2/s]
298	3.91	0.30	3.45	0.32
343	8.52	0.96	7.54	0.56
523	3.99	3.37	38.83	1.30
723	3.13	8.69	204.3	4.60

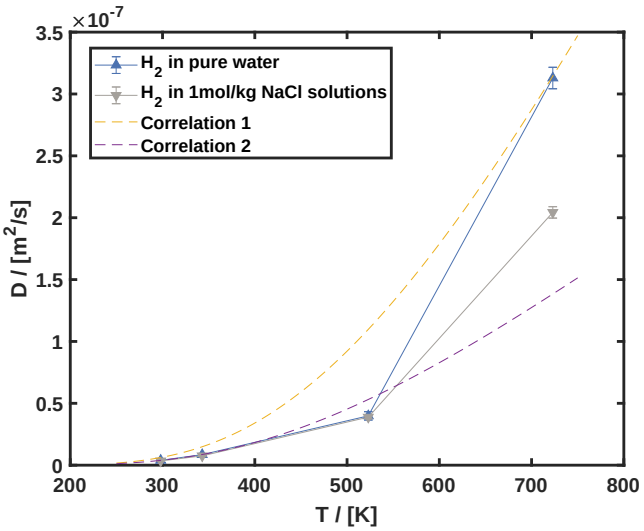

Figure 4.25: The results of the self-diffusion coefficient calculation for hydrogen at 298K in pure water and NaCl solutions under 400bar vs. temperature. Correlations 1 and 2 are fits to the experimental data in 1 bar[22]

The experimental fit in the figure comes from ref [22]. In this paper, the Arrhenius-type curves of D vs. temperature is created to describe the experimental data in 1 bar. The equation of the curve can be described as follows:

$$D = D_0 \exp\left(\frac{\alpha}{T}\right) \tag{4.1}$$

where D_0 and α are the fitting parameters. α in this case can be expressed as : $\alpha = \frac{-E_\alpha}{R}$, where E_α is the activation energy for diffusion and R is the universal gas constant. The detailed fitting parameters are shown in table 4.9.

Table 4.9: Parameters of the Arrhenius Fit (equation 4.1) to the Experimental Data of H_2 in H_2O at 1 Atm

	$ln(D_0)$	α
correlation 1	−12.22±0.48	(−0.199±0.014) × 10^4
correlation 2	−13.29±0.37	(−0.181±0.011) × 10^4

Although the fitting experimental curve is based on the 1 bar pressure, the diffusion coefficient of hydrogen does not change a lot as we can seen from the previous sections, the comparison of the experimental data and the 400bar simulation data still make sense. The results of the 400bar situations falls in-between the two curves means that the chosen forcefield is a good way to predict the diffusion coefficient of hydrogen in the solutions.

5

Conclusion

In this project, massive data for the density, shear viscosity and diffusion coefficient of hydrogen in NaCl solutions are provided, which greatly enriching the gaps in experimental results in this field. Based on the calculation of the transport properties of hydrogen in different molalities of the NaCl system, the method of the molecular dynamics simulations shows great agreement to the experimental results, with shorter time to obtain results, a wider range of experimental conditions and relatively ideal results.

The forcefield combining the TIP4P/2005 water model, the Vrabec hydrogen model and Madrid forcefield shows good agreement when calculating the transport properties. For the 0.85 forcefield, it is more suitable for the low molalities of the NaCl system while the 0.75 forcefield shows better performance in the high molalities, especially when calculating the shear viscosity of the whole aqueous solution system.

Temperature variations have a large influence on the system transport characteristics, but pressure changes have less impact. When the temperature increase, the density, shear viscosity of the whole system falls significantly. But with higher cohesive energy with the whole system, the diffusion coefficient increase. As the pressure varies, all of the transport properties change little.

When it comes to the diffusion coefficient of hydrogen in the systems, the presence of ions particles somehow reduces the coefficient compared to the pure water system. The Yeh−Hummer equation aids in the final results' agreement with the experimental data.

6

Recommendation

Limited by time, there is still a lot of work which related to this project can be done.

Forcefield selection
For the further investigation of the transport properties, the ions forcefield can be improved for better predicting the diffusion coefficient of different kinds of gases. Different kinds of ions forcefield can be selected and compared for a better prediction. The optimization of the forcefield is also needed to develop in the future. The other choice of one site hydrogen forcefield can also be considered for a better combination of the forcefield.

Wider temperature range
Since temperature of the whole system truly influences a lot in all the transport properties, more simulations under moderate temperatures between 343K to 523K can be done to create a predictable model to calculate the transport properties.

System exploration
Other cations and anions can also be added into the simulation system in order to be a better assumption as the condition which related to the underground hydrogen storage. For example, the system contains potassium ions, hydroxide ion and and other ions which is quite possible to be shown in the underground situations can be a good choice.

7

Acknowledgement

In successfully completing this project, many people have helped me. I would like to thank all those who are related to this project.

First of all, great appreciation to my supervisor Otto and Poulumi for their inspiration and meticulous review! Without their guide, I will never encounter such a beautiful field and will never finish this thesis. Also, great appreciate to Parsa who is so kind for helping me along all the journey in my thesis. You are all my enlightenment mentors! The suggestions and directions from yours have helped in the completion of this project.

I would also like to thank my parents and friends who have helped me with their valuable suggestions and guidance in these valuable two years. In particular, I strongly feel grateful to Siqi, Yue and Yufan who are always there to support me, with the vital help from the great friendship I really feel at home. The friendship that I created here in Delft with Fanhao is precious. Also, it is such a great honor for me to study with Jing and Yu during these two years in the materials science and engineering department. Likewise, thank you Yan and Pingyao for always being by my side. Also great thanks to Yibo Wang who is always insisting on his love which deeply inspired me to trace my own loved target in my life journey.

Last but not least, thank you all guys in the materials science and engineering department of Delft University of technology!

References

[1] Davood Zivar, Sunil Kumar, and Jalal Foroozesh. “Underground hydrogen storage: A comprehensive review”. In: *International Journal of Hydrogen Energy* 46.45 (2021). Hydrogen Separation, Production and Storage, pp. 23436–23462. ISSN: 0360-3199. DOI: https://doi.org/10.1016/j.ijhydene.2020.08.138. URL: https://www.sciencedirect.com/science/article/pii/S0360319920331426.

[2] Xin Liu, André Bardow, and Thijs J. H. Vlugt. “Multicomponent Maxwell−Stefan Diffusivities at Infinite Dilution”. In: *Industrial & Engineering Chemistry Research* 50.8 (2011), pp. 4776–4782. DOI: 10.1021/ie102515w. eprint: https://doi.org/10.1021/ie102515w. URL: https://doi.org/10.1021/ie102515w.

[3] Daan Frenkel and Berend Smit. “Introduction”. In: *Understanding Molecular Simulation (Second Edition)*. San Diego: Academic Press, 2002. ISBN: 978-0-12-267351-1. DOI: https://doi.org/10.1016/B978-012267351-1/50003-1. URL: https://www.sciencedirect.com/science/article/pii/B9780122673511500031.

[4] Steve Plimpton. “Fast Parallel Algorithms for Short-Range Molecular Dynamics”. In: *Journal of Computational Physics* 117.1 (Mar. 1995), pp. 1–19. DOI: 10.1006/jcph.1995.1039.

[5] Seyed Hossein Jamali et al. “OCTP: A Tool for On-the-Fly Calculation of Transport Properties of Fluids with the Order-n Algorithm in LAMMPS”. In: *Journal of Chemical Information and Modeling* 59.4 (2019). PMID: 30742429, pp. 1290–1294. DOI: 10.1021/acs.jcim.8b00939. eprint: https://doi.org/10.1021/acs.jcim.8b00939. URL: https://doi.org/10.1021/acs.jcim.8b00939.

[6] Seung-Kwon Seo, Dong-Yeol Yun, and Chul-Jin Lee. “Design and optimization of a hydrogen supply chain using a centralized storage model”. In: *Applied Energy* 262 (2020), p. 114452. ISSN: 0306-2619. DOI: https://doi.org/10.1016/j.apenergy.2019.114452. URL: https://www.sciencedirect.com/science/article/pii/S0306261919321403.

[7] J.B. Taylor et al. “Technical and economic assessment of methods for the storage of large quantities of hydrogen”. In: *International Journal of Hydrogen Energy* 11.1 (1986), pp. 5–22. ISSN: 0360-3199. DOI: https://doi.org/10.1016/0360-3199(86)90104-7. URL: https://www.sciencedirect.com/science/article/pii/0360319986901047.

[8] Steven Flesch et al. “Hydrogen underground storage—Petrographic and petrophysical variations in reservoir sandstones from laboratory experiments under simulated reservoir conditions”. In: *International Journal of Hydrogen Energy* 43.45 (2018), pp. 20822–20835. ISSN: 0360-3199. DOI: https://doi.org/10.1016/j.ijhydene.2018.09.112. URL: https://www.sciencedirect.com/science/article/pii/S0360319918329793.

[9] KH Coats and JG Richardson. “Calculation of water displacement by gas in development of aquifer storage”. In: *Society of Petroleum Engineers Journal* 7.02 (1967), pp. 105–112.

[10] Per Dannemand Andersen et al. “Final report of the roads2hycom project: fuel cells and hydrogen in a sustainable energy economy”. In: (2009).

[11] Ariel Pérez et al. “Patagonia wind-hydrogen project: underground storage and methanation”. In: *21st world hydrogen energy conference*. 2016.

[12] Dieter Pudlo et al. “The H2STORE Project: Hydrogen Underground Storage – A Feasible Way in Storing Electrical Power in Geological Media?” In: *Clean Energy Systems in the Subsurface: Production, Storage and Conversion*. Ed. by Michael Z. Hou, Heping Xie, and Patrick Were. Berlin, Heidelberg: Springer Berlin Heidelberg, 2013, pp. 395–412. ISBN: 978-3-642-37849-2.

[13] J. Simon, A.M. Ferriz, and L.C. Correas. “HyUnder – Hydrogen Underground Storage at Large Scale: Case Study Spain”. In: *Energy Procedia* 73 (2015). 9th International Renewable Energy Storage Conference, IRES 2015, pp. 136–144. ISSN: 1876-6102. DOI: https://doi.org/10.1016/j.egypro.2015.07.661. URL: https://www.sciencedirect.com/science/article/pii/S1876610215014290.

[14] D Pudlo and S Henkel. “H2STORE and HyINTEGER—Studies on the Effect of Hydrogen Storage in (PORE) Underground Gas Reservoirs—An Overview”. In: *Proceedings of the 3rd HIPS-NET Workshop, Brussels, Belgium, June*. 2016, pp. 23–24.

[15] Sriramoji Manohar, Danuta Puchalska, and Gordon Atkinson. “Pressure-volume-temperature properties of aqueous mixed electrolyte solutions: sodium chloride+ barium chloride from 25 to 140. degree. C”. In: *Journal of Chemical and Engineering Data* 39.1 (1994), pp. 150–154.

[16] D. Perry R. H.; Green. *Perry’s Chemical Engineers’ Handbook, 7th Edition*. 7th ed. McGraw Hill:New York, 1997.

[17] Tsuyoshi Yamaguchi. “Structural Origin of Shear Viscosity of Liquid Water”. In: *The Journal of Physical Chemistry B* 122.3 (2018). PMID: 29256609, pp. 1255–1260. DOI: 10.1021/acs.jpcb.7b10893. eprint: https://doi.org/10.1021/acs.jpcb.7b10893. URL: https://doi.org/10.1021/acs.jpcb.7b10893.

[18] CV Suryanarayana and VK Venkatesan. “The viscosity of concentrated aqueous solutions of sodium chloride”. In: *Transactions of the Faraday Society* 54 (1958), pp. 1709–1711.

[19] F. Llovell, R. M. Marcos, and L. F. Vega. “Free-Volume Theory Coupled with Soft-SAFT for Viscosity Calculations: Comparison with Molecular Simulation and Experimental Data”. In: *The Journal of Physical Chemistry B* 117.27 (2013). PMID: 23789584, pp. 8159–8171. DOI: 10.1021/jp401307t. eprint: https://doi.org/10.1021/jp401307t. URL: https://doi.org/10.1021/jp401307t.

[20] Sergio E. Quiñones-Cisneros et al. “General friction theory viscosity model for the PC-SAFT equation of state”. In: *AIChE Journal* 52.4 (2006), pp. 1600–1610. DOI: https://doi.org/10.1002/aic.10755. eprint: https://aiche.onlinelibrary.wiley.com/doi/pdf/10.1002/aic.10755. URL: https://aiche.onlinelibrary.wiley.com/doi/abs/10.1002/aic.10755.

[21] Xiaojing Wang, Yanling Chi, and Tiancheng Mu. “A review on the transport properties of ionic liquids”. In: *Journal of Molecular Liquids* 193 (2014), pp. 262–266. ISSN: 0167-7322. DOI: https://doi.org/10.1016/j.molliq.2014.03.011. URL: https://www.sciencedirect.com/science/article/pii/S0167732214001123.

[22] Ioannis N. Tsimpanogiannis et al. “Engineering Model for Predicting the Intradiffusion Coefficients of Hydrogen and Oxygen in Vapor, Liquid, and Supercritical Water based on Molecular Dynamics Simulations”. In: *Journal of Chemical & Engineering Data* 66.8 (2021), pp. 3226–3244. DOI: 10.1021/acs.jced.1c00300. eprint: https://doi.org/10.1021/acs.jced.1c00300. URL: https://doi.org/10.1021/acs.jced.1c00300.

[23] A. D. McNaught and A. Wilkinson. “Compendium of Chemical Terminology, 2nd ed. (the ”Gold Book”)”. In: *Blackwell Scientific Publications* (1997). URL: https://doi.org/10.1351/goldbook.S05582.

[24] J.-F. Danel, L. Kazandjian, and G. Zérah. “Numerical convergence of the self-diffusion coefficient and viscosity obtained with Thomas-Fermi-Dirac molecular dynamics”. In: *Phys. Rev. E* 85 (6 June 2012), p. 066701. DOI: 10.1103/PhysRevE.85.066701. URL: https://link.aps.org/doi/10.1103/PhysRevE.85.066701.

[25] J. L. F. Abascal and C. Vega. “A general purpose model for the condensed phases of water: TIP4P/2005”. In: *The Journal of Chemical Physics* 123.23 (2005), p. 234505. DOI: 10.1063/1.2121687. eprint: https://doi.org/10.1063/1.2121687. URL: https://doi.org/10.1063/1.2121687.

[26] Andreas Köster, Monika Thol, and Jadran Vrabec. “Molecular Models for the Hydrogen Age: Hydrogen, Nitrogen, Oxygen, Argon, and Water”. In: *Journal of Chemical & Engineering Data* 63.2 (2018), pp. 305–320. DOI: 10.1021/acs.jced.7b00706. eprint: https://doi.org/10.1021/acs.jced.7b00706. URL: https://doi.org/10.1021/acs.jced.7b00706.

[27] I. M. Zeron, J. L. F. Abascal, and C. Vega. “A force field of Li+, Na+, K+, Mg2+, Ca2+, Cl−, and SO42− in aqueous solution based on the TIP4P/2005 water model and scaled charges for the ions”. In: *The Journal of Chemical Physics* 151.13 (2019), p. 134504. DOI: 10.1063/1.5121392. eprint: https://doi.org/10.1063/1.5121392. URL: https://doi.org/10.1063/1.5121392.

[28] Miguel Angel González and José L. F. Abascal. “The shear viscosity of rigid water models”. In: *The Journal of Chemical Physics* 132.9 (2010), p. 096101. DOI: 10.1063/1.3330544. eprint: https://doi.org/10.1063/1.3330544. URL: https://doi.org/10.1063/1.3330544.

[29] Kenneth R. Harris and Lawrence A. Woolf. “Temperature and Volume Dependence of the Viscosity of Water and Heavy Water at Low Temperatures”. In: *Journal of Chemical & Engineering Data* 49.4 (2004), pp. 1064–1069. DOI: 10.1021/je049918m. eprint: https://doi.org/10.1021/je049918m. URL: https://doi.org/10.1021/je049918m.

[30] Thomas E. Markland, Scott Habershon, and David E. Manolopoulos. “Quantum diffusion of hydrogen and muonium atoms in liquid water and hexagonal ice”. In: *The Journal of Chemical Physics* 128.19 (2008), p. 194506. DOI: 10.1063/1.2925792. eprint: https://doi.org/10.1063/1.2925792. URL: https://doi.org/10.1063/1.2925792.

[31] V. Buch. “Path integral simulations of mixed para□D2 and ortho□D2 clusters: The orientational effects”. In: *The Journal of Chemical Physics* 100.10 (1994), pp. 7610–7629. DOI: 10.1063/1.466854. eprint: https://doi.org/10.1063/1.466854. URL: https://doi.org/10.1063/1.466854.

[32] Roger F. Cracknell. “Molecular simulation of hydrogen adsorption in graphitic nanofibres”. In: *Phys. Chem. Chem. Phys.* 3 (11 2001), pp. 2091–2097. DOI: 10.1039/B100144M. URL: http://dx.doi.org/10.1039/B100144M.

[33] Saman Alavi, J. A. Ripmeester, and D. D. Klug. “Molecular-dynamics study of structure II hydrogen clathrates”. In: *The Journal of Chemical Physics* 123.2 (2005), p. 024507. DOI: 10.1063/1.1953577. eprint: https://doi.org/10.1063/1.1953577. URL: https://doi.org/10.1063/1.1953577.

[34] D. Marx and P. Nielaba. “Path-integral Monte Carlo techniques for rotational motion in two dimensions: Quenched, annealed, and no-spin quantum-statistical averages”. In: *Phys. Rev. A* 45 (12 June 1992), pp. 8968–8971. DOI: 10.1103/PhysRevA.45.8968. URL: https://link.aps.org/doi/10.1103/PhysRevA.45.8968.

[35] Shuichi Nosé. “A unified formulation of the constant temperature molecular dynamics methods”. In: *The Journal of Chemical Physics* 81.1 (1984), pp. 511–519. DOI: 10.1063/1.447334. eprint: https://doi.org/10.1063/1.447334. URL: https://doi.org/10.1063/1.447334.

[36] William G. Hoover. “Canonical dynamics: Equilibrium phase-space distributions”. In: *Phys. Rev. A* 31 (3 Mar. 1985), pp. 1695–1697. DOI: 10.1103/PhysRevA.31.1695. URL: https://link.aps.org/doi/10.1103/PhysRevA.31.1695.

[37] William G. Hoover, Anthony J. C. Ladd, and Bill Moran. “High-Strain-Rate Plastic Flow Studied via Nonequilibrium Molecular Dynamics”. In: *Phys. Rev. Lett.* 48 (26 June 1982), pp. 1818–1820. DOI: 10.1103/PhysRevLett.48.1818. URL: https://link.aps.org/doi/10.1103/PhysRevLett.48.1818.

[38] H. J. C. Berendsen et al. “Molecular dynamics with coupling to an external bath”. English. In: *Journal of Chemical Physics* 81.8 (1984), pp. 3684–3690. ISSN: 0021-9606. DOI: 10.1063/1.448118.

[39] Carsten Kutzner et al. “Speeding up parallel GROMACS on high-latency networks”. In: *Journal of Computational Chemistry* 28.12 (2007), pp. 2075–2084. DOI: https://doi.org/10.1002/jcc.20703. eprint: https://onlinelibrary.wiley.com/doi/pdf/10.1002/jcc.20703. URL: https://onlinelibrary.wiley.com/doi/abs/10.1002/jcc.20703.

[40] S Plimpton. “Fast parallel algorithms for short-range molecular dynamics”. In: (). DOI: 10.2172/10176421. URL: https://www.osti.gov/biblio/10176421.

[41] Seyed Hossein Jamali et al. “Thermodynamic and transport properties of crown-ethers: Force field development and molecular simulations”. In: *The Journal of Physical Chemistry B* 121.35 (2017), pp. 8367–8376.

[42] In-Chul Yeh and Gerhard Hummer. “System-Size Dependence of Diffusion Coefficients and Viscosities from Molecular Dynamics Simulations with Periodic Boundary Conditions”. In: *The Journal of Physical Chemistry B* 108.40 (2004), pp. 15873–15879. DOI: 10.1021/jp0477147. eprint: https://doi.org/10.1021/jp0477147. URL: https://doi.org/10.1021/jp0477147.

[43] Othonas A. Moultos et al. “System-size corrections for self-diffusion coefficients calculated from molecular dynamics simulations: The case of CO2, n-alkanes, and poly(ethylene glycol) dimethyl ethers”. In: *The Journal of Chemical Physics* 145.7 (2016), p. 074109. DOI: 10.1063/1.4960776. eprint: https://doi.org/10.1063/1.4960776. URL: https://doi.org/10.1063/1.4960776.

[44] Miguel Angel González and José L. F. Abascal. “The shear viscosity of rigid water models”. In: *The Journal of Chemical Physics* 132.9 (2010), p. 096101. DOI: 10.1063/1.3330544. eprint: https://doi.org/10.1063/1.3330544. URL: https://doi.org/10.1063/1.3330544.

[45] Marc Laliberté and W. Edward Cooper. “Model for Calculating the Density of Aqueous Electrolyte Solutions”. In: *Journal of Chemical & Engineering Data* 49.5 (2004), pp. 1141–1151. DOI: 10.1021/je0498659. eprint: https://doi.org/10.1021/je0498659. URL: https://doi.org/10.1021/je0498659.

[46] Darren Rowland. *Density of NaCl(aq)*. [Online; accessed dd-mmm-yyyy]. 2021. URL: https://advancedthermo.com/electrolytes/density_nacl_jun2021.html.

[47] Joseph Kestin, H Ezzat Khalifa, and Robert J Correia. “Tables of the dynamic and kinematic viscosity of aqueous NaCl solutions in the temperature range 20–150 C and the pressure range 0.1–35 MPa”. In: *Journal of physical and chemical reference data* 10.1 (1981), pp. 71–88.

A

Codes

A.1. Simulation code

```
#####################################################
# EXAMPLE for using the OCTP plugin
#################### SETTING UP ####################
units real
dimension 3
newton on
boundary p p p
atom_style full

#################### VARIABLES ####################
variable Temp equal 298       # Temperature in K
variable Pres equal 1.0       # Pressure in atm.

variable RandomSeed equal 85 # The random seed for velocity
variable tstep equal 1.0      # 1fs
variable Ninptpre equal 10000 # Pre-initialize the NPT ensemble (very small timesteps)
variable Ninpt equal 50000    # Initialize the NPT ensemble
variable Npnpt equal 1000000   # Production in the NPT ensemble (volume)
variable Ninvtpre equal 10000 # Pre-initialize the NVT ensemble (very small timesteps)
variable Ninvt equal 50000    # Initialize the NVT ensemble
variable Npnvt equal 100000   # Production in the NVT ensemble (energy)
variable Nrun equal 10000000   # production in the NVE ensemble
variable Nf equal 10000       # Nfreq (fix ave/time and thermo)
variable Ne equal  10         # Nevery (fix ave/time)
variable Nr equal ${Nf}/${Ne} # Nrepeat (fix ave/time)
variable NBR equal ${Npnpt}/50 # Block averaging for density (NPT)
variable Nd equal ${Npnvt}/10 # Frequency of outputting positions of atoms in the NVT
    ensemble

variable nb equal 10          # Number of blocks (fix ordern)
variable nbe equal 20         # Number of block elements (fix ordern)
variable Nvisc equal 5        # Nevery for viscosity (fix ordern: sample data at (Nvisc*2))
variable Ncond equal 5        # Nevery for Tconductivity (fix ordern: sample data at (Ncond
    *2))
variable Ndiff equal 1000     # Nevery for diffusivity (fix ordern: sample data at (Ndiff))
variable Nwrit equal 100000   # Nwrite for transport properties (fix ordern: write every (
    Nwrit))

variable Nrdfe equal 100      # Nevery for RDF (fix ave/time)
variable Nrdfw equal 1000     # Nwrite for RDF (compute rdf/ext: write every (Nrdfw*Nrdfe))
variable binnum equal 2000    # Number of bins for RDF

#################### ATOM DEFINITION and FORCEFIELD ####################
read_data ./data.lmp                    # read the positions
include ./forcefield.data                 # read the force field

#################### INITIALIZATION ####################
# groups for the central atoms of water (O)
```

```
group wat type 1      # The Oxygen of WATER molecules
group Na type 3
group Cl type 4
group h type 5

# neigbor lists
neighbor 2.0 bin
neigh_modify every 1 delay 0 check yes

# velocity-Verlet integrator
run_style verlet

# minimizing the system using the conjugate gradient method
min_style cg
min_modify dmax 0.05
minimize 1.0e-6 1.0e-6 1000 10000
reset_timestep 0

# initializing velocities
velocity all create ${Temp} ${RandomSeed}

# rate of writing thermal properties to the log file
thermo ${Nf}

##################### 1) Initialize the NPT ensemble ####################
# applying the shake algorithm for rigid molecules and the NPT solver
fix constrain all shake 1.0e-6 1000 0 b 1 a 1
fix integrate all npt temp ${Temp} ${Temp} 10.0 iso ${Pres} ${Pres} 100.0
#fix integrate all rigid/npt/small molecule temp ${Temp} ${Temp} 100.0 iso ${Pres} ${Pres}
    1000.0


# Initializing the whole system with very small timesteps in the NPT ensemble
timestep 0.001
run ${Ninptpre}
timestep 0.01
run ${Ninptpre}
timestep 0.1
run ${Ninptpre}
timestep 0.2
run ${Ninptpre}
timestep 0.5
run ${Ninptpre}
reset_timestep 0

# continuing the initialization with the final value of timestep
unfix integrate
fix integrate all npt temp ${Temp} ${Temp} 100.0 iso ${Pres} ${Pres} 1000.0
#fix integrate all rigid/npt/small molecule temp ${Temp} ${Temp} 100.0 iso ${Pres} ${Pres}
    1000.0

timestep ${tstep}
run ${Ninpt}
reset_timestep 0

##################### 2) Obtaining average volume in NPT ######################
# Getting the average volume of the system
variable Volume equal vol
fix VoluAve all ave/time 1 ${Npnpt} ${Npnpt} v_Volume file volume.dat


# Thermo style for outputing system properties to the log file
thermo_style custom density
thermo_modify flush yes

variable Dens equal density
fix DensAve all ave/time 1 ${NBR} ${NBR} v_Dens file density.dat

run ${Npnpt}
reset_timestep 0

```

```
115 ##################### 3) Initializing the NVT ensemble ####################
116 # scaling the size of the system to the average volume
117 variable sidesize equal (f_VoluAve^(1.0/3.0))    # get the volume
118 variable xlow equal xlo
119 variable ylow equal ylo
120 variable zlow equal zlo
121 variable xhig equal (xlo+${sidesize})
122 variable yhig equal (ylo+${sidesize})
123 variable zhig equal (zlo+${sidesize})
124 change_box all x final ${xlow} ${xhig} y final ${ylow} ${yhig} z final ${zlow} ${zhig}
125 unfix DensAve
126 unfix VoluAve
127
128 # changing the ensemble to NVT
129 unfix integrate
130 fix integrate all nvt temp ${Temp} ${Temp} 100.0
131 #fix integrate all rigid/nvt/small molecule temp ${Temp} ${Temp} 100.0
132 # Initializing the whole system with very small timesteps in the NVT ensemble
133 timestep 0.001
134 run ${Ninvtpre}
135 timestep 0.01
136 run ${Ninvtpre}
137 timestep 0.1
138 run ${Ninvtpre}
139 timestep 0.2
140 run ${Ninvtpre}
141 timestep 0.5
142 run ${Ninvtpre}
143 reset_timestep 0
144
145 # continuing the initialization with the final value of timestep
146 timestep ${tstep}
147 run ${Ninvt}
148 reset_timestep 0
149
150 ##################### 4) Obtaining average total energy in NVT ######################
151 thermo_style custom temp pe ke etotal
152 thermo_modify flush yes
153
154 variable T1 equal temp
155 variable TE1 equal etotal
156 variable KE1 equal ke
157 variable PE1 equal pe
158 fix Tave1 all ave/time ${Npnvt} 1 ${Npnvt} v_T1
159 fix TEave1 all ave/time 1 ${Npnvt} ${Npnvt} v_TE1
160 fix KEave1 all ave/time ${Npnvt} 1 ${Npnvt} v_KE1
161 fix PEave1 all ave/time ${Npnvt} 1 ${Npnvt} v_PE1
162
163 dump trjectory all xyz ${Nd} movie.xyz
164 dump_modify trjectory element O H Na Cl Hvr
165
166 run ${Npnvt}
167 reset_timestep 0
168
169 undump trjectory
170
171 ##################### 3) Simulating in NVE ensmeble ######################
172 # Scaling the temperature (kinetic energy) according to the average total energy
173 variable TempNew equal (f_Tave1*(f_TEave1-f_PEave1)/(f_KEave1))
174 velocity all scale ${TempNew}
175
176 unfix Tave1
177 unfix TEave1
178 unfix KEave1
179 unfix PEave1
180 variable T1 delete
181 variable TE1 delete
182 variable KE1 delete
183 variable PE1 delete
184 variable TempNew delete
185
```

```
# computing average total energy, pontential energy, temperature, and pressure over time
variable TotEn equal etotal
fix TEAve all ave/time ${Ne} ${Nr} ${Nf} v_TotEn file TotalE.dat

variable PotEn equal pe
fix PEAve all ave/time ${Ne} ${Nr} ${Nf} v_PotEn file PotenE.dat

compute T all temp
fix TempAve all ave/time ${Ne} ${Nr} ${Nf} c_T file temperature.dat

compute P all pressure T
fix PressAve all ave/time ${Ne} ${Nr} ${Nf} c_P file pressure.dat


# computing self-diffusion and Onsager coefficients using the OCTP plugin
compute positions all position
fix f3 all ordern diffusivity ${Ndiff} ${Nwrit} c_positions nb ${nb} nbe ${nbe} file diffself
    .dat diffonsag.dat


# computing shear and bulk viscosities  using the OCTP plugin
fix f1 all ordern viscosity ${Nvisc} ${Nwrit} c_P nb ${nb} nbe ${nbe} file viscosity.dat


# computing thermal conductivity using the OCTP plugin
compute KE all ke/atom
compute PE all pe/atom
compute ST all stress/atom NULL virial
compute heatflux all heat/flux KE PE ST
fix f2 all ordern thermalconductivity ${Ncond} ${Nwrit} c_heatflux nb ${nb} nbe ${nbe} file
    tconductivity.dat


# computing the RDF for all group pairs
compute rdfs all rdf/ext Nbin ${binnum} Nwrite ${Nrdfw} file rdf.dat
fix f4 all ave/time 1 1 ${Nrdfe} c_rdfs

# Thermo style for outputing system properties to the log file
thermo_style custom step temp f_TempAve press f_PressAve pe ke etotal
thermo_modify flush yes
#thermo 1
run ${Nrun}

quit
```

A.2. Madrid2019 Forcefield data

```
mass 1 15.9994 # Ow
mass 2 1.00794 # Hw
mass 3 22.9897 # Na
mass 4 35.4527 # Cl
mass 5 2.01588  #Hvr

pair_style lj/cut/tip4p/long 1 2 1 1 0.1546 10.0
kspace_style pppm/tip4p 1.0e-5
pair_modify tail yes

#-----------------Combinations----------------------------
pair_coeff 1 1 0.1852 3.1589     # Ow-Ow
pair_coeff 1 2 0.0000 0.0000     # Ow-Hw
pair_coeff 1 3 0.1894 2.6084     # Ow-Na
pair_coeff 1 4 0.0148 4.2387     # Ow-Cl
pair_coeff 1 5 0.0974 3.0978     # Ow-Hvr

pair_coeff 2 2 0.0000 0.0000     # Hw-Hw
pair_coeff 2 3 0.0000 0.0000     # Hw-Na
pair_coeff 2 4 0.0000 0.0000     # Hw-Cl
pair_coeff 2 5 0.0000 0.0000     # Hw-Hvr

```

```
pair_coeff 3 3 0.3517 2.2174     # Na-Na
pair_coeff 3 4 0.3437 3.0051     # Na-Cl
pair_coeff 3 5 0.1343 2.6270     # Na-Hvr

pair_coeff 4 4 0.0184 4.6991     # Cl-Cl
pair_coeff 4 5 0.0307 3.8678     # Cl-Hvr

pair_coeff 5 5 0.0513 3.0366     # Hvr-Hvr

bond_style  harmonic
bond_coeff 1 1000 0.9572          # Ow-Hw

angle_style harmonic
angle_coeff 1 100 104.52          # H-O-H

set type 1 charge -1.1128        # O
set type 2 charge +0.5564        # OH
set type 3 charge +0.8500        # Na
set type 4 charge -0.8500        # Cl
```

A.3. Madrid0.75 Forcefield data

```
mass 1 15.9994 # Ow
mass 2 1.00794 # Hw
mass 3 22.9897 # Na
mass 4 35.4527 # Cl
mass 5 2.01588  #Hvr

pair_style lj/cut/tip4p/long 1 2 1 1 0.1546 10.0
kspace_style pppm/tip4p 1.0e-5
pair_modify tail yes

#-----------------Combinations----------------------------
pair_coeff 1 1 0.1852 3.1589     # Ow-Ow
pair_coeff 1 2 0.0000 0.0000     # Ow-Hw
pair_coeff 1 3 0.1895 2.3873     # Ow-Na
pair_coeff 1 4 0.0148 4.0763     # Ow-Cl
pair_coeff 1 5 0.0975 3.0978     # Ow-Hvr

pair_coeff 2 2 0.0000 0.0000     # Hw-Hw
pair_coeff 2 3 0.0000 0.0000     # Hw-Na
pair_coeff 2 4 0.0000 0.0000     # Hw-Cl
pair_coeff 2 5 0.0000 0.0000     # Hw-Hvr

pair_coeff 3 3 0.3517 2.2174     # Na-Na
pair_coeff 3 4 0.3437 2.5801     # Na-Cl
pair_coeff 3 5 0.1343 2.6270     # Na-Hvr

pair_coeff 4 4 0.0184 4.6991     # Cl-Cl
pair_coeff 4 5 0.0307 3.8678     # Cl-Hvr

pair_coeff 5 5 0.0513 3.0366     # Hvr-Hvr

bond_style  harmonic
bond_coeff 1 1000 0.9572          # Ow-Hw

angle_style harmonic
angle_coeff 1 100 104.52          # H-O-H

set type 1 charge -1.1128        # O
set type 2 charge +0.5564        # OH
set type 3 charge +0.7500        # Na
set type 4 charge -0.7500        # Cl
```

A.4. Simulation results

Table A.1: Simulation results for 523K and 723K for 0.85 madrid forcefield

P	T	m	ρ	σ_ρ	η	σ_η	D_w	$\sigma_{D\,w}$	$D_{\mathrm{Na}+}$	$\sigma_{D\,\mathrm{Na}+}$	$D_{\mathrm{Cl}-}$	$\sigma_{D\,\mathrm{Cl}-}$	D_{H}	$\sigma_{D\,\mathrm{H}}$
100	523	1	835.3	0.3256	0.1232	0.003362	2.572E-08	1.024E-10	1.519E-08	9.055E-11	1.809E-08	3.841E-10	4.195E-08	2.007E-09
100	523	3	905.6	0.5527	0.1546	0.003329	2.13E-08	6.198E-11	1.312E-08	2.652E-10	1.485E-08	1.463E-10	3.21E-08	3.231E-09
100	523	5	965.2	0.3081	0.1971	0.01288	1.792E-08	1.025E-10	1.131E-08	1.327E-10	1.258E-08	2.105E-10	3.187E-08	6.542E-10
100	523	8	1040	0.2792	0.2425	0.01297	1.454E-08	1.1E-10	9.528E-09	7.041E-11	1.019E-08	8.12E-11	2.67E-08	1.44E-09
400	523	1	863.5	0.174	0.1336	0.00137	2.451E-08	2.53E-10	1.511E-08	3.354E-10	1.797E-08	5.878E-10	3.883E-08	1.297E-09
400	523	3	930.8	0.1892	0.1637	0.001741	2.025E-08	1.06E-10	1.256E-08	1.58E-10	1.454E-08	1.428E-10	3.291E-08	5.502E-10
400	523	5	987.5	0.2575	0.1977	0.005161	1.72E-08	1.138E-10	1.113E-08	2.199E-10	1.213E-08	1.046E-10	2.962E-08	1.43E-09
400	523	8	1060	0.1272	0.2555	0.005101	1.396E-08	1.675E-10	9.285E-09	7.378E-11	9.873E-09	2.358E-11	2.401E-08	4.835E-10
1000	523	1	906.2	0.2345	0.148	0.009827	2.234E-08	1.627E-10	1.364E-08	2.215E-10	1.655E-08	6.03E-10	3.322E-08	5.788E-10
1000	523	3	969.4	0.2336	0.1828	0.005157	1.867E-08	4.686E-11	1.183E-08	1.697E-10	1.365E-08	1.642E-10	2.866E-08	1.341E-09
1000	523	5	1024	0.1172	0.2168	0.006517	1.594E-08	6.737E-11	1.043E-08	1.487E-10	1.172E-08	9.831E-11	2.415E-08	1.8E-09
1000	523	8	1093	0.2698	0.2785	0.01454	1.299E-08	9.906E-11	8.807E-09	7.49E-11	9.354E-09	1.747E-10	2.174E-08	1.606E-09
400	723	1	463.5	0.9837	0.0516	0.0001935	8.432E-08	7.601E-10	4.003E-08	1.182E-09	3.99E-08	5.587		

Table A.2: Simulation results for 298K and 343K for 0.85 madrid forcefield

P	T	m	ρ	σ_ρ	η	σ_η	D_w	$\sigma_{D\,w}$	$D_{\mathrm{Na}+}$	$\sigma_{D\,\mathrm{Na}+}$	$D_{\mathrm{Cl}-}$	$\sigma_{D\,\mathrm{Cl}-}$	D_{H}	$\sigma_{D\,\mathrm{H}}$
1	298	1	1034	0.3515	1.016	0.04931	2.036E-09	7.566E-12	1.112E-09	4.42E-11	1.422E-09	4.151E-11	3.862E-09	4.595E-10
1	298	3	1103	0.4803	1.428	0.08711	1.514E-09	2.216E-11	8.862E-10	3.003E-11	1.036E-09	3.926E-11	2.825E-09	2.65E-10
1	298	5	1164	0.5042	2.104	0.1336	1.13E-09	1.119E-11	6.369E-10	3.221E-11	7.905E-10	1.378E-11	2.227E-09	2.799E-10
1	298	8	1241	0.3419	3.604	0.3726	7.064E-10	7.801E-12	4.156E-10	7.961E-12	4.883E-10	1.572E-11	1.368E-09	1.69E-10
10	298	1	1034	0.2033	1.089	0.1173	2.02E-09	2.623E-11	1.131E-09	3.157E-11	1.437E-09	4.839E-11	3.617E-09	2.827E-10
10	298	3	1103	0.421	1.516	0.07878	1.518E-09	1.601E-11	8.438E-10	1.996E-11	1.064E-09	1.686E-11	2.957E-09	1.602E-10
10	298	5	1163	0.433	2.04	0.1333	1.132E-09	1.604E-11	6.474E-10	5.47E-12	7.923E-10	2.486E-11	2.075E-09	1.627E-10
10	298	8	1242	0.7578	3.57	0.1742	7.061E-10	5.861E-12	4.095E-10	8.129E-12	4.939E-10	5.21E-12	1.397E-09	1.223E-10
100	298	1	1038	0.2499	1.011	0.04685	2.032E-09	2.41E-11	1.138E-09	1.633E-11	1.422E-09	6.616E-11	3.846E-09	2.291E-10
100	298	3	1107	0.5278	1.426	0.026	1.526E-09	1.273E-11	8.532E-10	2.092E-11	1.091E-09	2.25E-11	2.896E-09	2.642E-10
100	298	5	1166	0.5832	2.139	0.1097	1.116E-09	1.121E-11	6.391E-10	1.085E-11	7.824E-10	2.393E-11	2.135E-09	1.063E-10
100	298	8	1242	0.7578	3.57	0.1742	7.061E-10	5.861E-12	4.095E-10	8.129E-12	4.939E-10	5.21E-12	1.397E-09	1.223E-10
400	298	1	1050	0.1382	0.9473	0.1069	2.069E-09	2.821E-11	1.133E-09	6.059E-11	1.452E-09	6.751E-11	3.446E-09	3.191E-10
400	298	3	1117	0.5551	1.402	0.1151	1.517E-09	1.99E-11	8.207E-10	2.75E-11	1.115E-09	2.97E-11	2.657E-09	2.29E-10
400	298	5	1177	0.5564	2.12	0.0731	1.105E-09	1.169E-11	6.307E-10	2.244E-11	7.67E-10	3.924E-11	2.053E-09	1.783E-10
400	298	8	1254	0.4958	3.91	0.4607	6.759E-10	6.76E-12	3.955E-10	8.567E-12	4.646E-10	1.245E-11	1.191E-09	5.57E-10
1000	298	1	1073	0.4518	1.018	0.03345	2.056E-09	9.083E-12	1.093E-09	7.999E-11	1.483E-09	3.034E-11	2.936E-09	4.386E-10
1000	298	3	1138	0.274	1.62	0.1832	1.483E-09	1.282E-11	8.108E-10	1.225E-11	1.081E-09	2.659E-11	2.13E-09	6.094E-10
1000	298	5	1196	0.4508	2.226	0.1438	1.07E-09	1.256E-11	5.98E-10	1.282E-11	7.553E-10	1.456E-11	1.742E-09	9.941E-11
1000	298	8	1272	0.407	3.921	0.1436	6.404E-10	4.735E-12	3.66E-10	5.596E-12	4.396E-10	8.077E-12	1.161E-09	2.58E-10
1	343	1	1011	0.2942	0.4659	0.01968	4.826E-09	2.076E-11	2.732E-09	1.663E-10	3.412E-09	7.871E-11	8.477E-09	3.518E-10
1	343	3	1075	0.3247	0.6392	0.02134	3.778E-09	2.432E-11	2.213E-09	1.283E-10	2.666E-09	7.098E-11	6.878E-09	3.554E-10
1	343	5	1132	0.3401	0.84	0.02486	2.994E-09	1.597E-11	1.858E-09	2.422E-11	2.184E-09	3.962E-11	5.16E-09	1.132E-10
1	343	8	1206	0.3002	1.238	0.05876	2.147E-09	7.47E-12	1.386E-09	1.625E-11	1.543E-09	3.373E-11	4.289E-09	2.587E-10
10	343	1	1011	0.09644	0.4791	0.02098	4.797E-09	5.259E-11	2.84E-09	1.095E-10	3.408E-09	3.189E-11	8.499E-09	4.538E-10
10	343	3	1076	0.264	0.6231	0.02604	3.787E-09	2.066E-11	2.299E-09	3.992E-11	2.732E-09	5.12E-11	6.874E-09	5.66E-10
10	343	5	1133	0.3733	0.8612	0.1	2.974E-09	5.119E-11	1.847E-09	4.406E-11	2.191E-09	4.368E-11	5.284E-09	3.403E-10
10	343	8	1207	0.3172	1.28	0.1331	2.138E-09	1.67E-11	1.37E-09	2.049E-11	1.557E-09	2.144E-11	3.87E-09	4.709E-10
100	343	1	1015	0.2713	0.4772	0.01811	4.79E-09	2.542E-11	2.794E-09	5.59E-11	3.476E-09	6.963E-11	8.25E-09	2.431E-10
100	343	3	1079	0.1432	0.651	0.05161	3.765E-09	4.537E-11	2.212E-09	8.037E-11	2.698E-09	6.607E-11	5.944E-09	8.076E-10
100	343	5	1137	0.322	0.8111	0.02467	2.982E-09	4.39E-11	1.855E-09	2.708E-11	2.199E-09	2.233E-11	5.104E-09	5.076E-10
100	343	8	1210	0.4563	1.226	0.0717	2.127E-09	2.764E-11	1.384E-09	2.945E-11	1.516E-09	4.359E-11	4.022E-09	2.654E-10
400	343	1	1028	0.1487	0.5057	0.06247	4.727E-09	7.677E-11	2.77E-09	6.399E-11	3.364E-09	2.486E-10	7.535E-09	5.661E-10
400	343	3	1092	0.09915	0.6538	0.04437	3.69E-09	2.477E-11	2.183E-09	3.126E-11	2.667E-09	4.599E-11	6.023E-09	5.508E-10
400	343	5	1148	0.1913	0.9207	0.1001	2.895E-09	3.842E-11	1.784E-09	5.608E-11	2.138E-09	2.458E-11	5.047E-09	5.496E-10
400	343	8	1221	0.2467	1.202	0.1291	2.082E-09	2.3E-11	1.342E-09	3.164E-11	1.504E-09	2.327E-11	3.55E-09	4.37E-10
1000	343	1	1051	0.1253	0.509	0.01313	4.602E-09	3.845E-11	2.707E-09	2.545E-11	3.451E-09	4.758E-11	6.671E-09	9.773E-10
1000	343	3	1113	0.2452	0.6705	0.05522	3.578E-09	3.925E-11	2.153E-09	4.78E-11	2.641E-09	3.976E-11	6.308E-09	8.055E-10
1000	343	5	1168	0.07092	0.8632	0.03816	2.821E-09	1.652E-11	1.749E-09	3.086E-11	2.118E-09	3.113E-11	4.345E-09	2.636E-10
1000	343	8	1240	0.1948	1.353	0.03653	1.969E-09	9.654E-12	1.258E-09	2.733E-11	1.444E-09	1.299E-11	3.238E-09	6.252E-10

Table A.3: Simulation results for 0.75 madrid forcefield

P	T	m	ρ	σ_ρ	η	σ_η	D_w	$\sigma_{D\,w}$	$D_{\mathrm{Na}+}$	$\sigma_{D\,\mathrm{Na}+}$	$D_{\mathrm{Cl}-}$	$\sigma_{D\,\mathrm{Cl}-}$	D_{H}	$\sigma_{D\,\mathrm{H}}$
1	298	5	1162	0.412	1.56	0.09781	1.4E-09	2.11E-11	9.22E-10	1.38E-11	1.07E-09	2.83E-11	2.49E-09	1.7E-10
1	298	8	1244	0.2701	2.362	0.3385	1.05E-09	1.1E-11	6.94E-10	1.34E-11	7.78E-10	2.03E-11	2.02E-09	1.77E-10
10	298	5	1162	0.4775	1.668	0.09894	1.39E-09	1.44E-11	8.78E-10	2.4E-11	1.07E-09	2.69E-11	2.88E-09	1.32E-10
10	298	8	1245	0.5108	2.187	0.1195	1.05E-09	1.26E-11	6.96E-10	1.82E-11	7.71E-10	2.48E-11	2.17E-09	5.72E-11
100	298	5	1166	0.5548	1.607	0.0681	1.4E-09	5.54E-12	8.89E-10	3.47E-11	1.04E-09	5.45E-11	2.06E-09	8.46E-10
100	298	8	1249	0.4696	2.253	0.1498	1.04E-09	9.49E-12	7.1E-10	1.29E-11	7.77E-10	2.59E-11	2.06E-09	1.58E-10
400	298	5	1179	0.4526	1.618	0.09375	1.41E-09	8.69E-12	9.15E-10	1.75E-11	1.08E-09	2.41E-11	2.61E-09	1.47E-10
400	298	8	1261	0.5764	2.189	0.2064	1.05E-09	9.68E-12	7.04E-10	1.77E-11	7.82E-10	1.1E-11	1.8E-09	3.03E-10
1000	298	5	1202	0.6194	1.548	0.04774	1.42E-09	1.11E-11	9.43E-10	1.97E-11	1.1E-09	3.38E-11	2.3E-09	1.46E-10
1000	298	8	1284	0.6152	2.233	0.167	1.05E-09	5.68E-12	7.1E-10	1.12E-11	8.16E-10	1.68E-11	1.78E-09	2.07E-10
1	343	5	1137	0.2894	0.6903	0.0169	3.43E-09	3.68E-11	2.24E-09	3.4E-11	2.64E-09	1.32E-10	6.24E-09	7.37E-10
1	343	8	1217	0.3664	0.9133	0.03774	2.69E-09	4.94E-12	1.8E-09	1.9E-11	2.01E-09	4.94E-11	4.94E-09	1.97E-10
10	343	5	1137	0.2622	0.673	0.02797	3.46E-09	2.8E-11	2.21E-09	6.68E-11	2.66E-09	1.88E-11	6.05E-09	5.31E-10
10	343	8	1217	0.2565	0.9536	0.0637	2.66E-09	3.26E-11	1.78E-09	3.72E-11	2.06E-09	2.15E-11	4.2E-09	1.13E-09
100	343	5	1141	0.2802	0.714	0.01968	3.4E-09	4.58E-11	2.24E-09	2.06E-11	2.68E-09	2.77E-11	6.35E-09	4.71E-10
100	343	8	1221	0.352	0.9049	0.03865	2.67E-09	1.26E-11	1.79E-09	1.7E-11	2.07E-09	4.11E-11	4.4E-09	1.01E-09
400	343	5	1154	0.3968	0.7061	0.03265	3.38E-09	6.55E-11	2.17E-09	6.58E-11	2.6E-09	3.31E-11	5.83E-09	3.8E-10
400	343	8	1234	0.361	0.9621	0.04431	2.62E-09	9.08E-12	1.77E-09	2.06E-11	2.01E-09	3.06E-11	4.84E-09	2.79E-10
1000	343	5	1178	0.2967	0.7415	0.05239	3.31E-09	3.71E-11	2.22E-09	3.53E-11	2.63E-09	3.15E-11	5.45E-09	2.58E-10
1000	343	8	1258	0.2812	1.011	0.07738	2.57E-09	1.77E-11	1.78E-09	3.16E-11	2E-09	4.36E-11	4.17E-09	6.35E-10
100	523	5	966.5	0.506	0.1815	0.01084	1.94E-08	1.98E-10	1.21E-08	3.77E-10	1.39E-08	2.05E-10	3.42E-08	5.46E-10
100	523	8	1047	0.2009	0.2168	0.006076	1.62E-08	9.46E-11	1.04E-08	6.61E-11	1.15E-08	1.5E-10	2.89E-08	1.28E-09
400	523	5	992	0.169	0.1926	0.00872	1.84E-08	1.72E-10	1.17E-08	6.33E-11	1.33E-08	8.51E-11	3.12E-08	7.65E-11
400	523	8	1071	0.4356	0.2226	0.006048	1.54E-08	4.09E-11	1.02E-08	2.45E-10	1.1E-08	2.45E-11	2.64E-08	1.28E-09
1000	523	5	1033	0.1724	0.1957	0.003794	1.71E-08	9.23E-11	1.13E-08	1.24E-10	1.3E-08	2.45E-10	2.65E-08	9.29E-10
1000	523	8	1110	0.359	0.2507	0.009333	1.43E-08	8.05E-11	9.58E-09	7.17E-11	1.05E-08	9.42E-11	2.3E-08	1.5E-09
400	723	5	662.5	0.8831	0.07959	0.0021	5.67E-08	1.19E-10	3.08E-08	3.01E-10	3.21E-08	5.9E-10	1.24E-07	2.93E-10
400	723	8	771.4	0.5475	0.09876	0.001092	4.68E-08	2.46E-10	2.59E-08	1.75E-10	2.68E-08	5.97E-11	9.64E-08	2.48E-10
1000	723	5	802.2	0.5847	0.1057	0.003365	4.38E-08	2.17E-10	2.65E-08	2.35E-10	2.81E-08	3.2E-10	8.06E-08	2.33E-09
1000	723	8	886.7	1.011	0.1261	0.001897	3.76E-08	3.71E-10	2.3E-08	2.4E-10	2.42E-08	3.77E-10	6.56E-08	2.59E-09